Distribution Agreement

In presenting this thesis as a partial fulfillment of the requirements for a degree from Emory University, I hereby grant to Emory University and its agents the non-exclusive license to archive, make accessible, and display my thesis in whole or in part in all forms of media, now or hereafter know, including display on the World Wide Web. I understand that I may select some access restrictions as part of the online submission of this thesis. I retain all ownership rights to the copyright of the thesis. I also retain the right to use in future works (such as articles or books) all or part of this thesis.

Brantley Holland April 3rd 2020

Functional Analysis and Classification of Missense Mutations within a Critical Region of *GRIN2A*

By

Brantley Holland

Stephen F. Traynelis, PhD

Advisor

Neuroscience and Behavioral Biology, Emory University

Stephen F. Traynelis, PhD

Advisor

Keith Easterling, PhD

Committee Member

Astrid Prinz, PhD

Committee Member

Matthew Weinschenk, PhD

Committee Member

2020

Functional Analysis and Classification of Missense Mutations within a Critical Region of *GRIN2A*

by

Brantley Holland

Stephen F. Traynelis, PhD
Advisor

An abstract of
a thesis submitted to the Faculty of Emory College of Arts and Sciences
of Emory University in partial fulfillment
of the requirements of the degree of
Bachelor of Science with Honors

Neuroscience and Behavioral Biology

2020

Abstract

Functional Analysis and Classification of Missense Mutations within a Critical Region of *GRIN2A*

By Brantley Holland

NMDA receptors (NMDARs) are a subset of ligand gated ion channels glutamate receptors which are crucial for proper neural functioning. Mutations in the genes which encode for this receptor are associated with neurological disorders such as epilepsy, developmental delay and aphasia. In this paper we evaluate the functional consequences missense mutations within a highly conserved region of the gene encoding for the GluN2A subunit (*GRIN2A*) have on normal receptor functional. This region was identified by the Missense Tolerance Ratio and has a history of patent reported pathogenic variants. I catalog the spectrum of functional perturbations resulting from missense mutations in these regions in hopes of bringing clarity to the functional spectrum by defining the direction and the magnitude of these changes. Lastly, I classify these variants according to the guidelines for sequence variants interpretation laid out by the American College of Genomic Medicine.

Functional Analysis and Classification of Missense Mutations within a Critical Region of *GRIN2A*

By

Brantley Holland

Dr. Stephen Traynelis

Adviser

A thesis submitted to the Faculty of Emory College of Arts and Sciences
of Emory University in partial fulfillment
of the requirements of the degree of
Bachelor of Science with Honors

Department of Neuroscience and Behavioral Biology

2020

Acknowledgements

I would like to thank Dr. Stephen Traynelis and Dr. Scott Myers for their mentorship over the past two years and for their guidance on this project.

Additionally, I would like to thank James Allen for his guidance and friendship during my time at CFERV. Thank you for your teaching me the experimental methods and for your help during every part of this project. I would also like to specifically acknowledge your assistance with oocyte recordings where you helped me collect data on >1000 oocytes.

Lastly, I would like everyone at CFERV, Sukhan Kim, Dan Teuscher, and Lingling Xi for the help and support they gave me during my time with them.

Table of Contents

Introduction and Background

Glutamatergic System:

Glutamate (L-Glutamate), a small amino acid neurotransmitter, is the most common excitatory neurotransmitter in both the central and peripheral nervous system, with >90% of the brains synapses releasing glutamate (Attwell and Laughlin, 2001). In the central nervous system, glutamate pathways are involved in neural functions such as memory consolidation, neural communication, and motor coordination (Swanson et al., 2005). Glutamate pathways in the peripheral nervous system are involved in somatosensory and taste sensation, cardiac rhythmicity, and somatic cell communication (Niswender and Conn, 2010; Fernández-Montoya et al., 2018; Chen and Kukley, 2020). Glutamate synapses are tightly regulated by more than 30 membrane-bound transporters and receptor proteins that are expressed in both neuronal and glial cells (Figure 1). This regulatory system is responsible for fine-tuning glutamate pathways by modulating synaptic and post-synaptic glutamate levels, neuronal excitability, and synaptic firing rates of neurons (Kandel et al., 2000; Kumar, 2015).

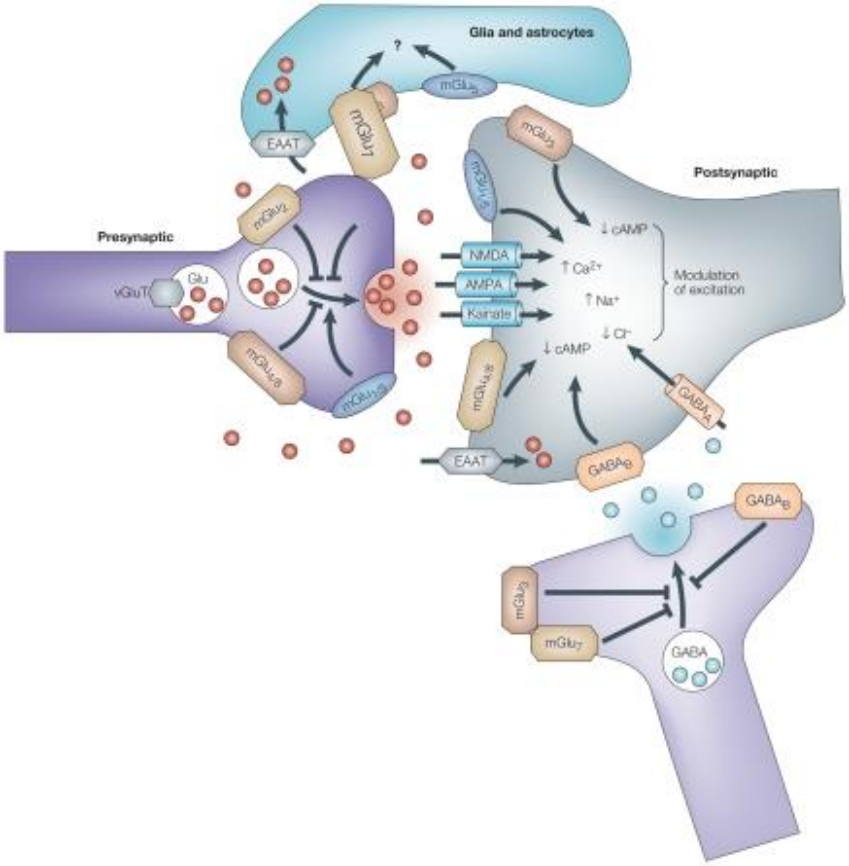

Figure 1. A hypothetical glutamatergic synapse showing presynaptic transmission of glutamate, glutamate transporters and receptors, as well as the diversity of postsynaptic responses glutamate can elicit.(Courtesy: Swanson et al., 2015)

Perturbations to glutamate pathways or their regulatory systems are associated with many neurological and psychiatric disorders (Swanson et al., 2005; Papouin et al., 2012; Fernández-Marmiesse et al., 2019).

Metabotropic Glutamate Receptors:

Glutamate receptors are transmembrane receptor proteins whose primary endogenous agonist is L-Glutamate (Traynelis et al., 2010). There are two classes of glutamate receptors: metabotropic glutamate receptors (mGluR) and ionotropic glutamate receptors (iGluR). Metabotropic glutamate receptors are G-protein-couple receptors (GPCRs) that are responsible for a large portion of glutamate's physiological functions (Niswender and Conn, 2010; Grados et al., 2015; Fernández-Montoya et al., 2018). mGluRs use diverse sets of electrical and chemical pathways to modulate ion channel properties and expression patterns, regulatory protein activity levels, and intracellular messenger systems (Anwyl, 1999; Coutinho and Knöpfel, 2002; Niswender and Conn, 2010). These pathways involve large numbers of molecules that can remain active for well over a minute and induce changes in distant regions of the cell, enabling glutamate to induce large-scale spatial and temporal changes (Kandel et al., 2000). The exact physiological mechanisms through which these effects take place are poorly understood. However, the primary mechanism is as follows: glutamate binds to the extracellular domain of mGluRs, initiating a conformational cascade which propagates through the receptor's transmembrane domains to a large intracellular domain. This intracellular domain contains a C-terminus that is responsible for modulating G-protein coupling and initiating cell signaling pathways (Niswender and Conn, 2010).

mGluRs are encoded for by eight genes (GRM1-GRM8), resulting in eight distinct mGluR subunit types (GRM1-GRM8). mGluR subunit types are grouped into three groups (Group I-Group III) based on their sequence homology, G-protein coupling, and ligand selectivity (Niswender and Conn, 2010). These groups also share similarities in their localization and general physiological function(Chen and Kukley, 2020). Within the central nervous system, Group I mGluRs (mGluR1/5) are predominantly expressed at postsynaptic and extrasynaptic sites within neurons and are associated with post-synaptic specialization of glutamate synapses (Ménard and Quirion, 2012). Group II mGluRs (mGluR2/3) is primarily expressed on the presynaptic terminal of excitatory synapses where they are involved in dampening neuronal excitability by inhibiting glutamate release through Long-Term Depression (LTD) (Grueter and Winder, 2005). Group III mGluRs (mGluR4/6/7/8) are commonly co-expressed with mGluR2/3 on the presynaptic terminal and have been shown to inhibit glutamate release at excitatory-inhibitory and excitatory-neuromodulatory synapses, allowing them to modulate a diverse set of neuronal functions (Chen and Van Den Pol, 1998; Nicoletti et al., 2011).

Ionotropic Glutamate Receptors:

Ionotropic glutamate receptors are tetrameric assemblies of modular subunits that dimerize to form large cation-selective ligand-gated ion channels (Dingledine et al., 1999; Hansen et al., 2010). iGluRs are voltage-dependent ion channels

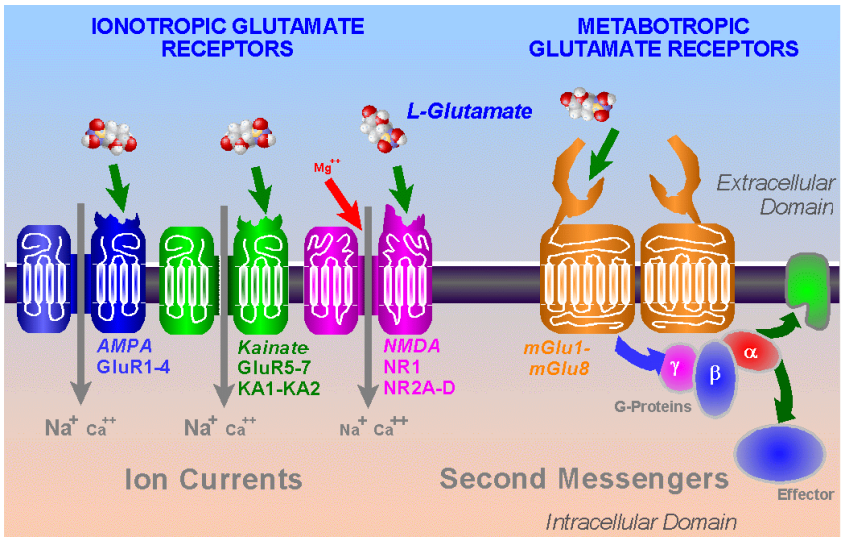

Figure 2: Ionotropic and metabotropic glutamate receptors (Courtesy of ucl.ac.uk)

that transfer positive currents across cellular membranes(Skowrońska et al., 2019). iGluRs are responsible for the majority of fast excitatory synaptic transmission within the nervous system and are associated with nearly all aspects of nervous system function and development (Coutinho and Knöpfel, 2002; Traynelis et al., 2010). iGluRs are expressed on neuronal and non-neuronal cells throughout the brain, spinal cord, and peripheral nervous system, where they mediate a broad spectrum of neurological processes (Traynelis et al., 2010; Hogan-Cann and Anderson, 2016; Chen and Kukley, 2020). Within the central nervous system, iGluRs play an essential role in sensory perception, learning and memory consolidation, motor coordination, and neuronal plasticity (Hollmann, 1994; Amin et al., 2017). Peripherally expressed, iGluRs are known to regulate cardiac rhythmicity, tumor proliferation, and nociceptive pathways (Toft, 2014; Hogan-Cann and Anderson, 2016). iGluR subtypes share a high degree of structural and sequence homology but have diverse pharmacological, kinetic, and functional profiles (Hansen et al., 2010).

All iGluR subunits contain four structural domains: an extracellular amino-terminal domain (ATD), an extracellular ligand-binding domain (LBD), a transmembrane domain (TMD), and an intracellular carboxyl-terminal domain (CTD) (Figure 3) (Traynelis et al., 2010). The ATD of iGluRs contains several binding sites for divalent cations, extracellular proteins, and allosteric modulators (Traynelis et al., 2010). The ATD plays a role in subunit dimerization and receptor formation through a series of complex subunit-subunit interactions(Yi et al., 2018). The LBD of these subunits is highly conserved across the iGluR class and governs a variety of receptor functions such as activation kinetics, agonist selectivity, and subunit dimerization (Hansen et al., 2010; Amin et al., 2017). The LBD also contains each subunit’s agonist binding

site. The TMD of all iGluR subtypes consists of three transmembrane alpha-helices (M1, M3, and M4) and a non-membrane spanning pore loop (M2) (Traynelis et al., 2010). The TMDs connect to the LBD through three short domain linkers (Černý et al., 2019). Upon subunit assembly, the TMDs define the ion channel pore of iGluRs, the region responsible for determining ion-channel selectivity (Lee et al., 2014; Amin et al., 2017). The CTD is a large intracellular domain that is important in receptor expression regulation, but the structural and functional resolution of iGluR's CTD area remains poor (Gill et al., 1998; Coutinho and Knöpfel, 2002). These four domains are largely autonomous though each contains sites where subunit-subunit interactions can occur (Dingledine et al., 1999; Li et al., 2019). Inter-subunit interactions occur upon receptor assembly and involve domain interactions such as TMD-LBD interactions, resulting in observed subunit cooperativity (Traynelis et al., 2010).

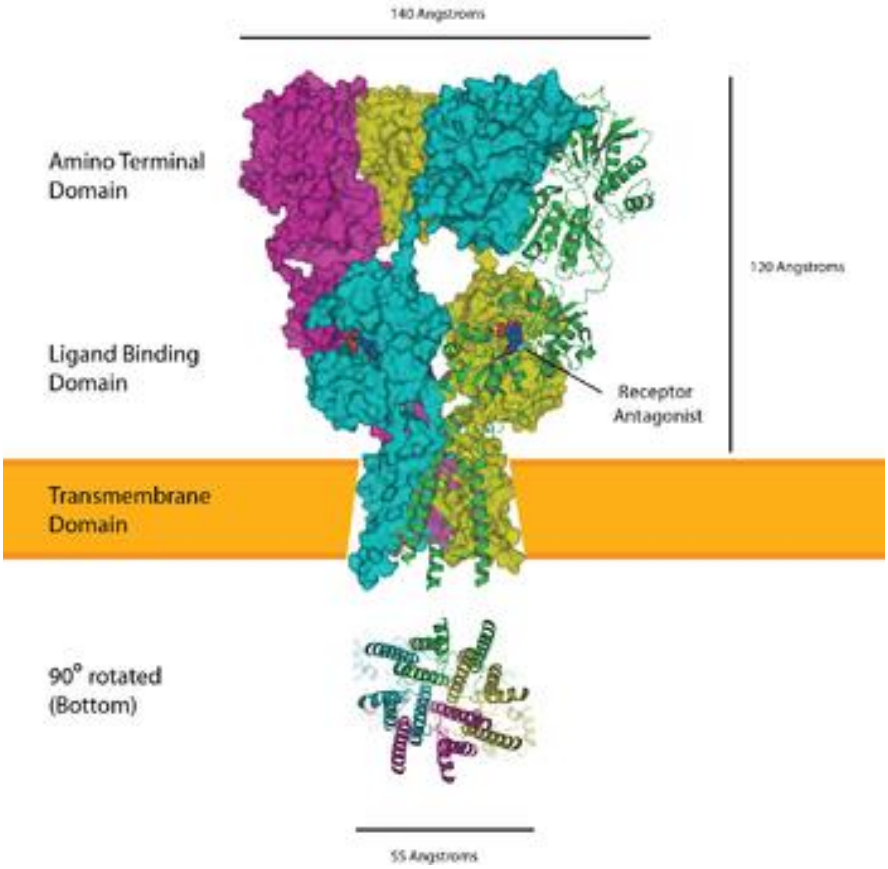

Figure 3: AMPA Receptor displaying the 4 protein domains and their location within the membrane (Courtesy: Curtis Neveu)

Within the iGluR class, there are three pharmacologically defined families: AMPA, kainate, and NMDA receptors (Figure 2). Each receptor family is named after an agonist

selective for their receptor family (Dingledine et al., 1999). α-amino-3-hydrox-5-methyl-4-isoxazolepropionic acid receptors (AMPAR) are heterotetrameric receptors formed by four distinct subunits (GluA1-GluA4) (Squire, 2010; Amin et al., 2017). AMPA receptors are expressed on the membrane of neurons and glial cells, but 60%-70% of AMPA receptors can be found within intracellular regions (Squire, 2010). AMPARs are distributed widely throughout the brain, and their expression is temporally and spatially regulated (David Weaver et al., 1996; Cull-Candy et al., 2006). AMPARs have activation/deactivation times on the order of milliseconds and are responsible for glutamates rapid postsynaptic potentials (Clements et al., 1998). Their fast kinetics make them keen targets for modulating neuronal excitability and plasticity. Kinetic profiles vary within the AMPAR family (Jonas, 2000). This diversity is achieved through the regulation of the synaptic density of AMPARs and changes in AMPAR subunit composition (David Weaver et al., 1996; Cull-Candy et al., 2006). AMPAR expression is activity-dependent and occurs within rapid time frames (Cull-Candy et al., 2006). AMPA expression is intimately linked to subunit composition, which dictates receptor trafficking modes and biophysical properties such as calcium permeability (Cull-Candy et al., 2006; Li et al., 2019b). Many developmental disorders are associated with disruptions in neuronal plasticity, making AMPAR induced plasticity of intense interest to researchers (Hollmann, 1994; Cull-Candy et al., 2006; Lapidus et al., 2013). Despite this, subunit expression is poorly cataloged, and regional and spatial resolution of these processes remain poor (Cull-Candy et al., 2006).

Kainate receptors are the least understood family of iGluRs (Niciu et al., 2012). They are referred to as AMPA's cousins, but research into their diverse physiological functions continues to differentiate them from AMPA (Niciu et al., 2012). Kainate receptors are tetrameric receptors formed through the assembly of five possible subunits (GluK1-5) (Alt et al., 2004). Kainate receptors are expressed widely throughout the brain, though their temporal and regional expression patterns remain unclear, in part due to the low selectivity of pharmacological tools used to differentiate receptor subtypes (Alt et al., 2004). Kainate receptors exhibit remarkably plastic functional profiles that are highly dependent on receptor subunit composition and subcellular location (Hollmann, 1994; Squire, 2010). Postsynaptic kainate receptors have various kinetic properties, allowing them to produce both rapid and slow excitatory post-synaptic currents (Vesikansa et al., 2012; Akgül et al., 2016). Though they are excitatory receptors, presynaptic kainate receptors produce powerful inhibitory effects on neurotransmitter release through the use of slow kinetic profiles, which result in periods of prolonged depolarization, depleting presynaptic terminals of glutamate and preventing the disinhibition of voltage-gated calcium channels (Chittajallu et al., 1996).

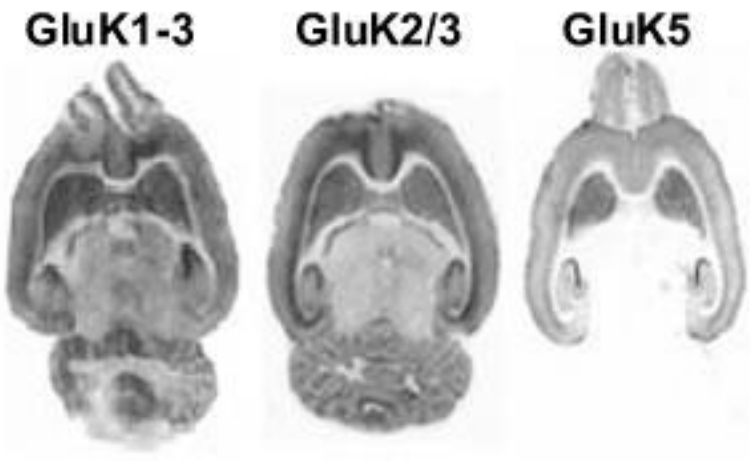

Figure 4: Distribution of Kainate Receptor Subunits in Adult Rat Brain (Courtesy: (bristol.ac.uk/)

NMDA Receptors:

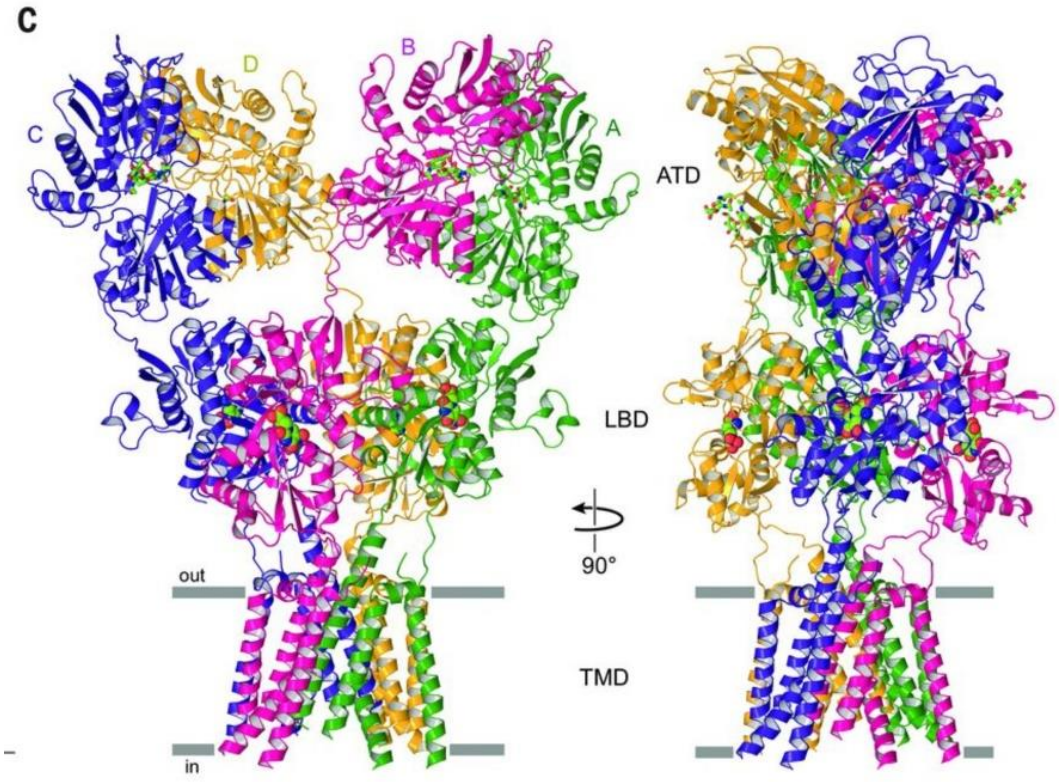

Figure 5: GluN2A NMDA receptor protein structure with and without agonist and co-agonist bound, showing the conformational changes induced by agonist binding (Yelshanskaya et al., 2014).

N-methyl-D-aspartate receptors (NMDAR) are a family of ionotropic glutamate receptors critical for proper neurological functioning (Li et al., 2019a). NMDARs are tetrameric glutamate ion channels that mediate glutamate's slow excitatory potentials (Myers et al., 2019). These receptors have slow kinetic profiles, high permeability to $Ca^{++,}$ and produce the most robust post-synaptic potentials of all iGluRs (Traynelis et al., 2010). They exhibit diverse pharmacological, structural, and functional profiles which are dependent on their subunit composition and regional expression(Vyklicky et al., 2018). NMDARs are active only in the presence of an agonist (L-glutamate) and a co-agonist (glycine/D-serine) (Monyer et al., 1994; Yi et al., 2018). NMDAR's are regulated by a diverse set of endogenous allosteric modulators such as Zn^{++}, polyamines, and H^{+}(Karakas et al., 2009; Li et al., 2019b). NMDARs are expressed throughout the central nervous system, where they mediate neural functions such as synaptic plasticity, neural communication, and memory formation (Shohami and Biegon, 2014; Akgül et al., 2016; Myers et al., 2019). These receptors have been implicated in several developmental, motor, neurodegenerative, and learning disorders (Traynelis et al., 2010; Hogan-

Cann and Anderson, 2016). NMDARs also show dynamic expression in response to traumatic brain injuries and ischemic stroke, suggesting a possible role in recovery from these events (Carvajal et al., 2016). Their diverse functional profiles are endowed by their structural and pharmacological properties (Rojas and Dingledine, 2013). NMDARs are unique among iGluRs in that they are modulated by extracellular Mg^{++}, which acts as a channel blocker at resting membrane voltages, preventing ion flow in polarized cells (Kandel et al., 2000). These positive ions are attracted to the strongly negative interior of NMDARs ion channel and are involved in producing NMDARs voltage-dependent gating properties (Monyer et al., 1992). These gaiting properties are the basis for basic model synaptic plasticity models such as Hebbian learning and Long-Term Potentiation (LTP).

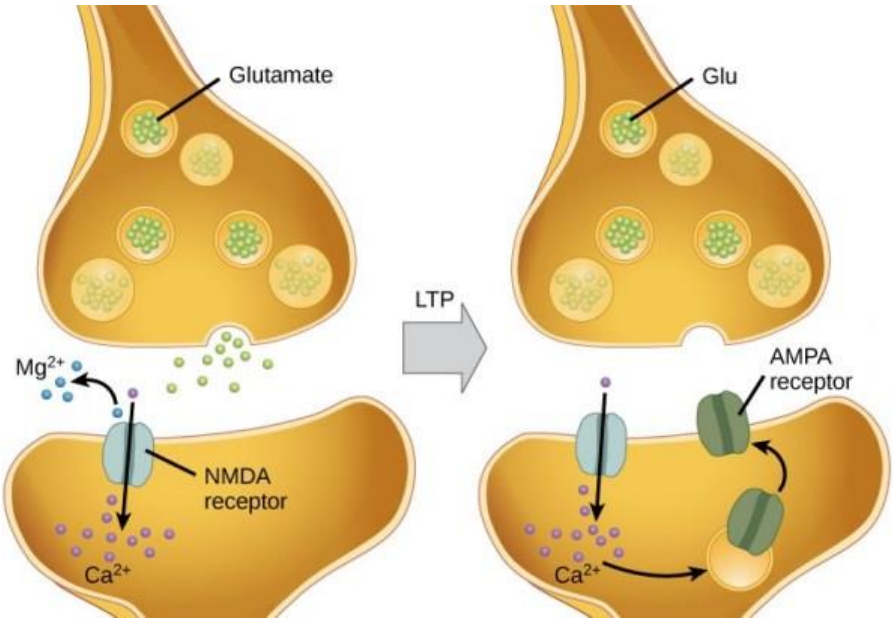

Figure 6: showing the mechanism of Long-Term Potentiation occurring at a glutamatergic synapse (Courtesy: OpenStax College)

NMDAR Subunit Variability

Functional NMDARs are comprised of four modular subunits which, based on sequence homology, have been categorized into three subfamilies: GluN1-GluN3 (Traynelis et al., 2010). The GluN1 subfamily is encoded for by a single gene (*GRIN1*), which, through RNA alternative splicing, can be expressed as eight distinct isoforms (Yi et al., 2018). The GluN2 subfamily contains four subunits (GluN2A-GluN2D), each encoded for by individual genes (*GRIN2A*-

GRIN2D) (Traynelis et al., 2010). Two GluN3 subunits are also expressed (GluN3A/GluN3B) and are also each encoded by individual genes (*GRIN3A*/*GRIN3B*) (Pérez-Otaño et al., 2016). GluN1 subunits are expressed ubiquitously in NMDARs, and assemblies with GluN2 subunits constitute the vast majority of NMDA receptors found within the nervous system. GluN1 subunits contain NMDARs glycine agonist binding site while GluN2 subunits contain NMDARs glutamate binding sites, making these receptors unique among the iGluRs class in that they are active only in the presence of an agonist (L-glutamate) and a co-agonist (glycine/D-serine) (Papouin et al., 2012; Myers et al., 2019; Wu et al., 2019).

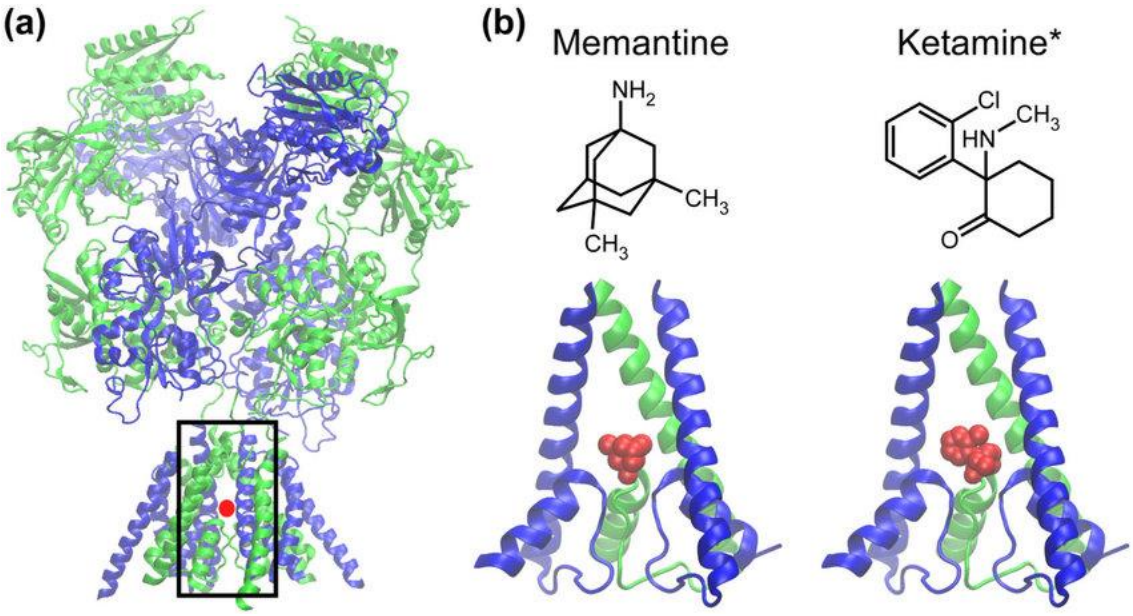

Figure 5: Two FDA approved compounds, Memantine and Ketamine act as pore blockers for NMDARs in a similar way to magnesium ions. Memantine is a drug approved for use in dementia patients to help improve memory and awareness. Ketamine is frequently used as an anesthetic and is currently in clinical trials for use as an antidepressant.

Kinetic, pharmacological, and expression profiles of NMDARs vary with subunit composition and are a source of the NMDARs diverse functional profile (Iacobucci and Popescu, 2018). GluN2 subunits contain important allosteric binding sites for ligands, such as Zn^{++} and H^{+} (Traynelis and Cull-Candy, 1990; Karakas et al., 2009). These modulators can have dramatic effects on NMDARs function, with nearly 50% of GluN1/GluN2A receptors being inhibited at physiological pH (Traynelis and Cull-Candy, 1990). These modulators are released in an

activity-dependent manner from pre-synaptic glutamate neurons and may play a neuroprotective role against glutamate excitotoxicity during ischemic strokes and seizures (Karakas et al., 2009). Glutamate, glycine, and allosteric modulator potency vary depending on the receptor's subunit composition, with glycine binding potency varying 8-fold between GluN2 subunit types (Zhou and Sheng, 2013).

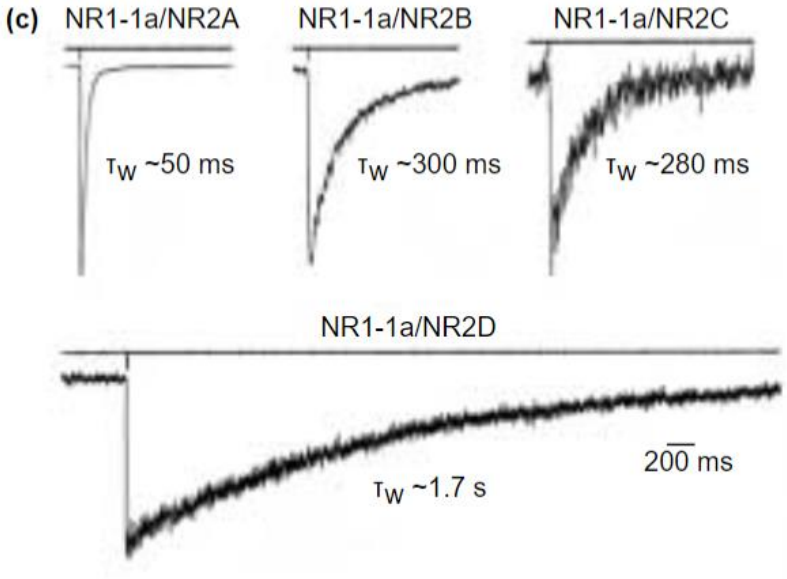

Figure 6: Macroscopic currents recorded from HEK293 cells expressing recombinant NMDA receptors with GluN2A, GluN2B, GluN2C and GluN2D subunits. Kinetic profiles of each receptor are responsible for the different time courses shown in this figure. Tw represents a weight average of each receptor type's deactivation time constant. (Vicini et al., 1998)

NMDARs have the slowest kinetic profiles of iGluRs with activation times measured in milliseconds and dissociation times in the tens to hundreds of milliseconds (Traynelis et al., 2010). Subunit composition endows receptors with their kinetic profiles (Figure 6). GluN2A containing receptors have faster kinetics than GluN2B, resulting in GluN2B transferring around twice the amount of depolarizing charge than GluN2A (Iacobucci and Popescu, 2018). Changes in activation and deactivation of receptors allow them to mediate different neurological processes and is intimately linked with their gating mechanisms (Iacobucci and Popescu, 2018; Černý et al., 2019). A receptors gating mechanism is a complex process involving both chemical and physical forces, which results in the opening and closing of the ion channel. It begins with agonist binding to the LBD, which causes "clam-shell" structures to fold over the agonist, inducing conformational changes in the extracellular domain (Figure 5) (Traynelis et al., 2010). These conformational changes are then transmitted to anchor points within the membrane via

rotations of the LBD-TMB linkers, resulting in channel opening (Černý et al., 2019). Variance in these processes is linked to changes in the receptor's kinetic profile, allowing neurons to change the magnitude and time-courses of NMDA mediated post-synaptic potentials by varying subunit expression (Figure 6) (Yi et al., 2018).

The functional consequences of GluN1 isoforms remain mostly unknown, with only limited kinetic differences in GluN1/GluN2D receptors having been reported (Swanger et al., 2015). GluN1 isoforms do not exhibit effects on the pharmacological or kinetic profile of NMDARs when combined with other subunits (Yi et al., 2018). The splicing events target the C- and N- terminus of the GluN1 subunit, regions associated with the binding and recognition of surface trafficking proteins, making it likely that these events affect receptor trafficking and expression profiles instead (Coutinho and Knöpfel, 2002; Yi et al., 2018). These profiles play a crucial role in facilitating NMDARs physiological effects (Monyer et al., 1994). The expression patterns of GluN2 vary across development, and these changes coincide with neurological developmental milestones. Phenotypes caused by perturbations or mutations affecting only one subunit type often follow similar courses of development, which coincide with their expression pattern (Figure 7) (Myers et al., 2019). Together with the pharmacological and kinetic profiles of NMDARs, their expression patterns show how NMDARs can mediate such diverse neurological functions.

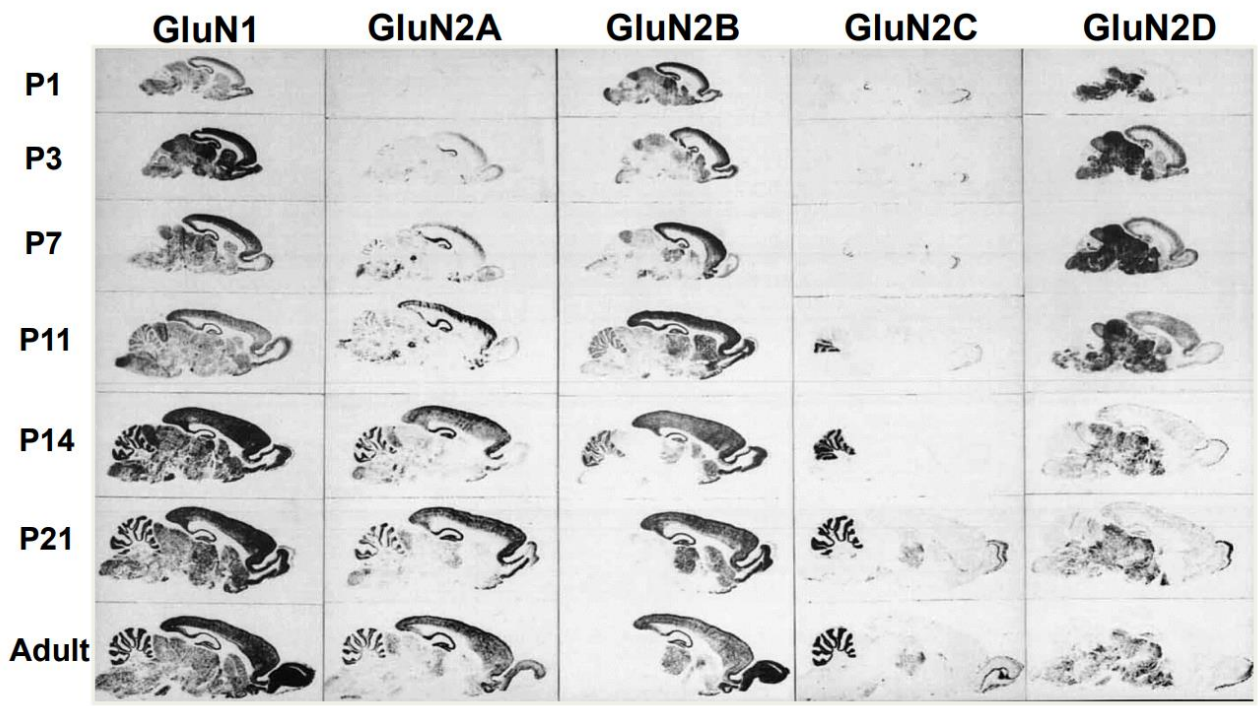

Figure 7: Negative film showing the expression profile of NMDARs in Rattus norvegicus brain and how it varies by subunit composition. Several developmental landmarks correspond with changes in subunit composition, such as the development of several reflexes on P7, and walking on P14 (Akazawa et al., 1994).

Genomic Sequencing:

Genetic sequencing is the process of determining the nucleotide sequence of DNA. The first genetic sequencing methods, such as the Sanger and Maxam-Gilbert method, were developed in the 1970s and required researchers to manually read individual nucleic acids in a DNA sequence through incredibly laborious processes (Toft, 2014). These methods remained the standard until the advent of automated sequencing methods in the 1990s (Dewey et al., 2012). Automated sequencing dramatically increased the capabilities of researchers by allowing them to sequence large DNA strands in a fraction of the time required for manual methods(Davies, 2013). This new technology helped to illuminate a significant source of disease: genetic mutations (Kwon and Goate, 2000). Previous to the 1990s, pedigree studies were the only way that researchers were able to identify the genetic component of diseases (Carvill et al., 2013; Bomba et al., 2017). With the large amount of genomic data made available by automated sequencing methods, researchers began to better correlate disease states with genetic data (Traynelis et al., 2017). However, the high costs associated with this technology and the lack of genomic reference data limited its application (Davies, 2013; Toft, 2014). The publication of the Human Genome Project in 2001 gave researchers their first reference sequence, allowing them to better correlate genetic variance with disease states (Hamosh et al., 2000; Jimenez-Sanchez et al., 2001). The Human Genome Project significantly contributed to the reduction in the operating costs, increasing the accessibility of high-throughput genetic sequencing technology (Davies, 2013). Since then, over 1000 genes associated with diseases, so-called disease genes, have been identified within the human genome (Jimenez-Sanchez et al., 2001). Clinical application of this technology and its findings have the potential to drastically reduce healthcare costs, increase diagnostic speed and accuracy, and improve patient care (Dewey et al., 2012).

Despite the potential of this technology, next-generation sequencing technology has failed to become routine in clinical care (Toft, 2014). Two major factors prevent the routine use of next-generation sequencing technology in clinical settings: data validation and data interpretation. High throughput sequencing error rates (>0.1%) are too high for clinical standards, meaning clinically significant variants must be verified using manual methods which have far lower error rates (~0.001%) (Dewey et al., 2012). Improvements in methodology and sequencing algorithms have failed to bring these error rates down to clinically useful levels. While the accuracy of manual sequencing methods has improved over the last decade, the cost, and most importantly, time, required have since plateaued (Ma et al., 2019). The reliance on more costly and time-consuming sequencing methods for data validation has restricted genomic sequencing to later in the diagnosis process, where its impact on healthcare costs and expediency is far less significant (Toft, 2014).

A second challenge lies in interpreting the genetic information obtained from patients. Genetic variance can result in pathogenic phenotypes and is the source of many disorders, but identifying what variation is responsible for this has proven to be extremely difficult (Bomba et al., 2017). Many tools, databases, and methods have been developed aimed at making sense of this variance, but the consequences of the vast majority of human genetic variance remain poorly understood (Traynelis et al., 2017).

Several organizations have attempted to standardize variant interpretation in order to improve geneticist's ability to identify deleterious genetic variation. One comes from the American College of Medical Genetics (ACMG), who has given a framework for how to characterize genetic variants as either pathogenic or benign variants. This framework operates by categorizing, weighing, and combining information on variants within disease genes to provide a

variant classification of benign, likely benign, uncertain significance, likely pathogenic or pathogenic. The ACMG lays out five categories of variant data: Population Data, Variant Type, Clinical Observations, Experimental Studies, and Indirect/Computational prediction. Data points gathered from these categorizes are then characterized as either pathogenic or benign based on various lines of evidence laid out by the ACMG (Supplemental Table 1). For evidence suggesting variant pathogenicity, the ACMG provides four evidence weights: very strong (PVS), strong (PS), moderate (PM), and supporting (PP). Evidence suggesting variant benignity is categorized by significance of the evidence into three categories: stand-alone, (BA1), strong (BS), and supporting (BP). Weighted data points are then combined to classify variants as either: benign, likely benign, uncertain significance, likely pathogenic, or pathogenic according to the thresholds laid out in Figure 8 (Richards et al., 2015).

Experimental Rational:

This thesis focuses on the affect's missense mutations within the human *GRIN2A* gene have on NMDA receptor function. It seeks to categorize and classify the functional effects of missense mutations across 14 amino acid residues 808-821 within the GluN2A NMDAR subunit. These residues were chosen because of their known roles in regulating key receptor properties as well as their history of pathogenic missense mutations. The first nine amino acid residues (808-816) compose the last sequence of a linker, which connects the agonist binding domain with the M4 domain of the GluN2A NMDAR subunit. In assembled NMDARs, this pre-M4 linker resides near two receptor gating domains of neighboring GluN1 subunits. The first is a highly conserved sequence motif within the M3 domain of GluN1 subunits, which controls the gating of the NMDARs. The second is a small pre-M1 helix, which acts to stabilize the receptor's closed state. In addition, several pathogenic variants within this linker have been reported in patients

with devastating effects. These include S809R, L812M, I814T, and D815E. The last five amino acid residues (817-821) make up the first residues of the last GluN2A transmembrane domains, M4. This region interacts with two transmembrane helices of adjacent GluN1 subunits in assembled NMDA receptors. This region is also highly conserved and contains two amino acids (M817 and V820) of a sequence motif known as MVGLAVE (Figure 9). Moreover, five possible pathogenic variants have been identified within this sequence: M817V, M817R, M817T, A818T, and A818E.

I seek to characterize the functional effects of missense variants within this highly conserved region in order to gain a better understanding of the functional spectrum caused by missense mutations within conserved regions of the *GRIN2A* gene. Conserved regions of *GRIN2A* are known to be important for proper protein function; however, the spectrum of functional perturbations resulting from missense mutations in these regions has not been thoroughly cataloged. I hope to bring clarity to this functional spectrum by defining the direction and the magnitude of these changes. In addition, I will classify these variants according to the guidelines for sequence variants interpretation laid out by the American College of Genomic Medicine in an attempt to assess the diagnostic capabilities of the Missense Tolerance Ratio, a missense variant-specific diagnostic tool.

This thesis also hopes to layout recommendations for a pragmatic approach to analyzing missense variants before they are reported within a patient population. Rare and pathogenic variants are being reported in disease genes every day, and there is a need to categorize these variants before they are reported in patients. Identifying the regions where pathogenic variants are likely to occur and categorizing them before they are reported is one way of getting ahead of the patient genomic data constantly flowing in from clinics. Due to this region’s proximity to

genetic motifs, clinical history, and sequence homology, I hypothesize that a majority of these variants will result in pathogenic phenotypes.

American College of Genomic Medicine Evidence Categories:

Population Data:

Population data is collected using large, publicly available population databases such as ClinVar (ncbi.nlm.nih.gov/clinvar) and gnomAD (gnomad.broadinstitute.org). Data from these sources is used to create allelic frequencies, which can be used to inform clinicians on the likelihood that a variant is pathogenic. For instance, higher than normal allelic frequencies, in patient population databases such as ClinVar or lower than normal allelic frequencies in control populations support a pathogenic variant interpretation. If, however, a variant has an allelic frequency >5% frequency in a control population database such as gnomAD, then that variant cannot consider as a pathogenic variant. For variants below this threshold, an average frequency within control populations observed alongside a low allelic frequency within patient populations support a benign interpretation of the variant.

It should be noted that this kind of population information is not always available, and its significance should be considered within the context of other variant information. In particular, variant penetrance, the rate at which pathogenic variants result in disease states, is an important factor to consider alongside population data. A low variant penetrance can result in pathogenic variants that exhibit average allelic frequencies in control populations. Unfortunately, data on variant penetrance is not always available and is only available for the most well-studied disease gene (Duzkale et al., 2013). In addition, datasets such as gnomAD suffer from sampling errors,

which result in diseased individuals being improperly included in the gnomAD dataset (Karczewski et al., 2019). These sampling errors are a result of several factors that are difficult to identify correctly. For these reasons, a full understanding of the disease biology of pathogenic variants is helpful in cases where variant population data may present conflicting lines of evidence.

Variant Type/Loci:

The second source of variant information comes from assessments of variant types. Variant type is a broad category that encompasses many different aspects, such as mutation type (missense, null, frameshift, synonymous, etc…) and the location of a mutation. Basic ideas from biology can be applied to the definition of variant type as well as historically reported clinical or functional data. For example, the ACMG considers variants resulting in dramatically altered sequences such as null or frameshift mutations to be more deleterious than mutations that result in single amino acid changes such as missense mutations (Jimenez-Sanchez et al., 2001). These mutation types can be further characterized based on their location, with truncating and frameshift mutations occurring in the beginning portions of a gene being considered more likely to cause a pathogenic phenotype than those occurring within later portions of the gene, as these earlier mutations result in a far more altered gene product (Lek et al., 2016). The importance of variant location for missense or synonymous mutation is more nuanced and requires further analysis. One way the ACMG suggests interpreting the impact of a missense mutation loci is through its proximity to previously reported pathogenic variants. If, for instance, a variant occurs at the same amino acid as an established pathogenic variant, the chances of that variant resulting in a pathogenic increase (Richards et al., 2015).

Many missense mutations reported in patients do not enjoy the support of this kind of historical data, in which case other criteria must be used to establish the importance of a missense mutation's loci. One of these is regionally observed genetic variance. If a missense mutation occurs within a region of the human genome with little or no genetic variance, then it is more likely to result in a pathogenic phenotype than one occurring in a region with high levels of variance (Chuang and Li, 2004). This has led the ACMG to give extra weight to missense mutations that occur within conserved genetic sequences. The most extreme example of genetic conservation occurs in regions known as sequence motifs. These are regions of genes whose amino acid sequence is shared between distantly related clades (Amin et al., 2017). Such motifs are the result of strong purifying natural selection, which has been established as a useful criterion with which to infer the biological importance of genetic regions (Chang and Kuo, 2008). Missense mutations within highly conserved regions such as genetic motifs are frequently reported in patient populations (Chang and Kuo, 2008; Strehlow et al., 2019)

Observing the connection between regional genetic variation and pathogenic variants, a team of researchers from the Melbourne School of Medicine created a diagnostic tool aimed at better cataloging regional variation in well-studied disease genes, in hopes of providing a better way of assessing the importance of a missense mutation's loci. This tool is known as the Missense Tolerance Ratio (MTR), and it seeks to quantify the amount of purifying selective pressure occurring within small amino acid sequences of genes. This was done by calculating theoretical missense mutation rates of small genetic sequences and comparing these rates to observed missense mutation rate using this equation:

$$\mathrm{MTR} = \frac{[\mathrm{missense[obs]}/(\mathrm{missense[obs]} + \mathrm{synonymous[obs]})]}{[\mathrm{missense[\,pos]}/(\mathrm{missense[\,pos]} + \mathrm{synonymous[\,pos]})]},$$

If no purifying selection is occurring in these regions, then the ratio of observed and theoretical mutation rates should be near 1. Disparities from this value can then be used to quantify the amount of purifying selection occurring with these regions. MTR values are reported for individual amino acid residues within well-studied disease genes and were used to create maps that show a gene's regional tolerance to missense mutations (Figure 8). The use of purifying selective pressure to infer biological significance in this way has proven to be useful and aligns well with clinically reported pathogenic missense variants (Figure 8). MTR values can be used in conjunction with the ACMG framework, which suggests that genetic variants occurring with critical regions have a higher likelihood of resulting in pathogenic phenotypes.

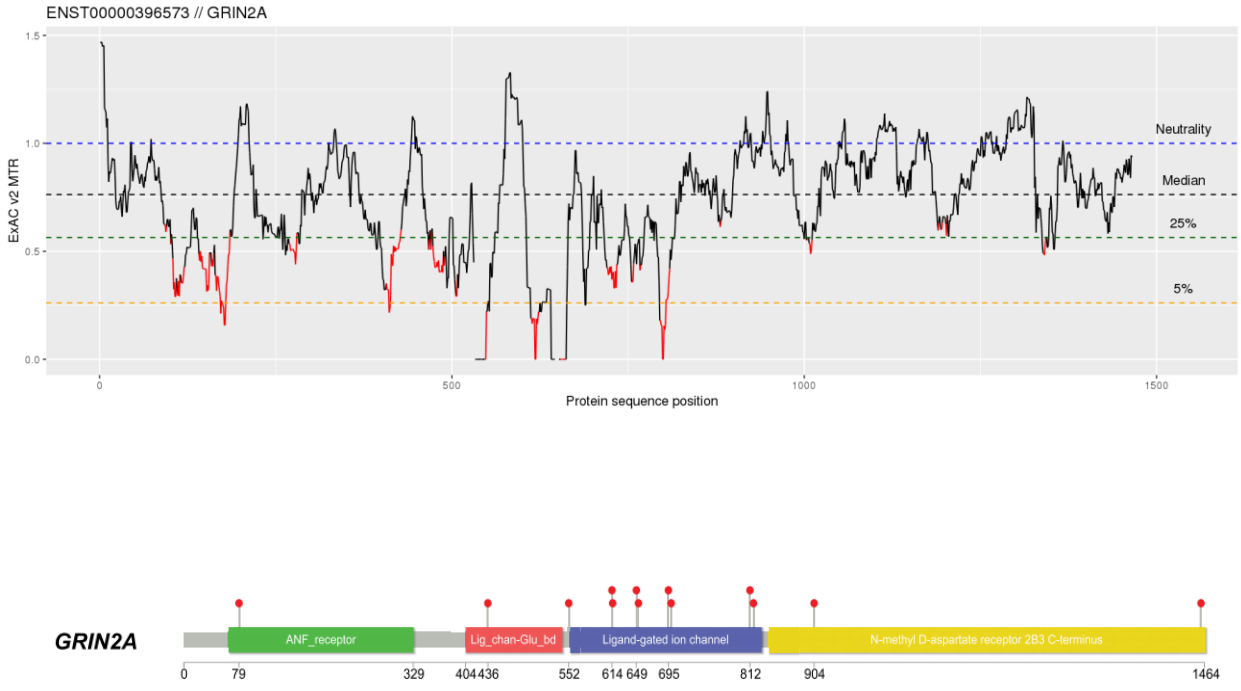

Figure 8: MTR map of GRIN2A is shown above a gene map showing patient reported pathogenic variants on a map of GRIN2A. In addition the functional domains of GluN2A receptors encoded for by GRIN2A is shown. Portion of the MTR in red received a study-wide false discovery rate of <0.05. Each red dot represents a patient reported variant (Courtesy: Traynelis et al., 2017)

Clinical Observations:

The third category of information recommended by the ACMG for the interpretation of pathogenic variants is clinical observations. Clinically derived data can include simple clinical observations such as clinical diagnosis, the age of onset of a disorder, symptom/phenotypic displays, and family history. Information such as the prevalence of a disorder or disease penetrance is also included in this category. The availability and accuracy of clinical observation vary between genes or disease type, and few cases will have access to all possible clinically obtainable data. Things such as disease prevalence, disease penetrance, or modes of inheritance are often difficult to gather either due to lack of data or lack of resources to examine individual cases properly. Although this clinical data serves to inform the other ACMG data categories. For example, the mode of inheritance informs variant penetrance, which in turn can help inform the significance of observed allelic frequencies. Other sources of data, such as disease etiology, can strengthen the predictive power of clinical data correspondingly. If, for instance, a disease affecting development is reported alongside a genetic variant that is involved in movement disorders, it is less likely that this variant is the cause of the developmental disorder. If, however, a variant occurs within a gene whose product is known to be involved in proper neurological development, then the likelihood that this variant is the source of the developmental disorder increases.

Experimental Studies/Functional Data:

The fourth data category used in assessing variant pathogenicity is experimental or functional data. Experimentally derived data is a potent but indirect source of information about variant pathogenicity. This data can come from cellular, animal, or molecular studies and generally involves the assessment of possible pathomechanisms of genetic disorders. For this

reason, experimental studies do not directly answer the question of whether a variant is pathogenic or not. Rather, it uses inferences from observed perturbations to systems known to be involved in the production of disease states and assesses the possibility that these changes would result in a pathogenic phenotype. Making definitive correlations between this data and pathogenicity is difficult, especially for those diseases where an understanding of the disease biology is poor. Establishing the threshold of perturbations that result in a pathogenic phenotype continues to be a barrier to the implementation of this data. It is a major reason the ACMG limits the use of functional analysis to the well-established means of analysis, though little detail as to what is considered well established is provided by the ACMG variant interpretation guidelines.

At the present moment, there are no cures for genetic disorders, and the management of presentations is the only course of action available to clinicians. As described by the ACMG, variant interpretation is a process that assesses the casual relationship of genetic variants and disease states. However, functional analysis studies have the ability to go beyond establishing what is, or is not, pathogenic and may begin to establish the underlying pathomechanisms of a genetic disease such as pathomechanisms. An understanding of how altered gene products produce disease states can serve to inform clinical decision making and patient care.

In-silico Modeling

The last data category established by the ACMG is also the least impactful. This data comes from computational predictions or *in silico* modeling. This type of assessment uses computational and protein models to infer the effects of non-synonymous mutations by analyzing the changes in gene products produced by specific mutations. Some models do this through the use of protein crystallization structures and protein functional studies to assess the likelihood that a variant is pathogenic. These models are useful in that they can inform clinicians quickly and

cheaply, but this data is only not the most accurate and is only used as supporting evidence for variant classification.

Figure 9: MVGLAVE sequence motif shown for NMDA and AMPA genes (Amin et al., 2017)

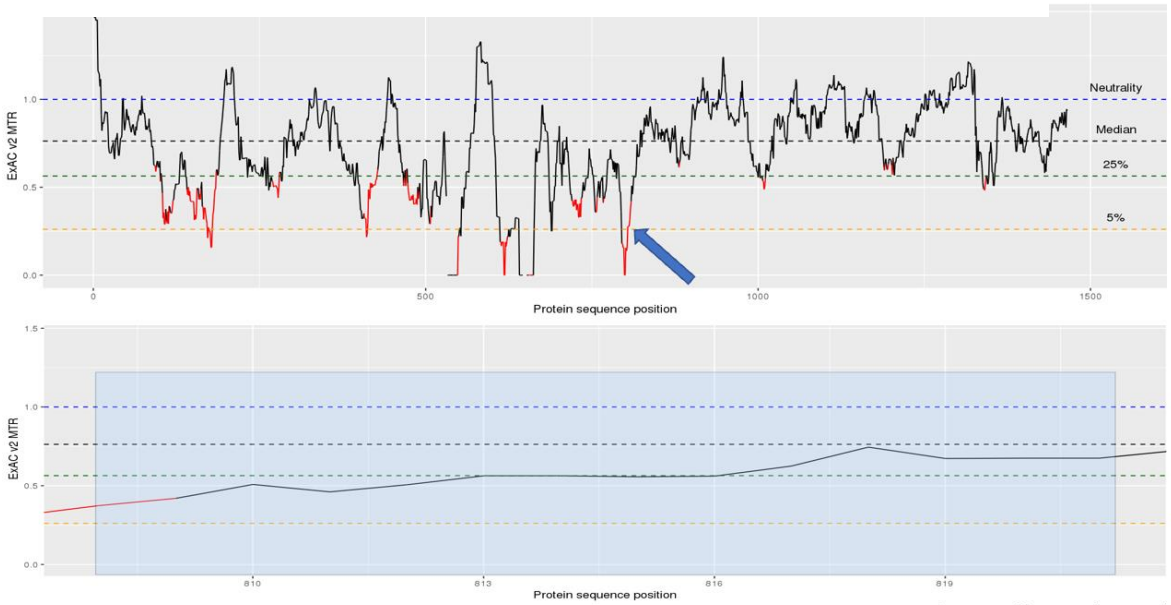

(Traynelis et. al, 2017)

Figure 10 The MTR gene map for GRIN2A is shown with the blue arrow pointing to the location of AA 808-821. Below is shown a zoomed in portion AA 808-821's positon within this map.

Materials and Methods:

Variant Interpretation:

The variant interpretation process was conducted using the framework laid out by the ACMG. First population data on variants occurring within AA 808-821 of the *GRIN2A* gene was gathered from ClinVar and gnomAD. All variants in this study are single nucleotide missense mutations, and so variant loci were assessed using the MTR diagnostic tool. The proximity to other clinically reported pathogenic variants was also used in the assessment of variant loci. Available clinical data was gathered from on variants from this region, which were reported in ClinVar. Information such as resultant disease states or modes of inheritance were not available for the vast majority of surveyed variants though a brief overview of the clinical presentations of *GRIN2A* variants is provided. Lastly, the functional analysis of these variants was conducted to assess their pharmacological profiles. No *in silico* models were used in the interpretation process.

Variant Determination:

All possible amino acid variants resulting from a single base pair change at each amino acid residue 808-821 in the *GRIN2A* gene were determined. All possible variants were then organized into separate files based on amino acid residue position. Each variant within these files was then randomly assigned a number from 1 up to 7 using Excel 2016's random number generator. Groups of variants, each containing one variant per residue, were then created by matching their numbers assigned by the random number generator. The first three files created in this manner were then selected as the 42 variants for study. Any variant resulting in a stop codon was replaced by the next variant in line.

This type of variant selection is unique to this project. Several other projects have sought to classify and define possible pathogenic mutations before using functional evaluation, but none to my knowledge have done this by restricting themselves to single base pair change variants. This is an important distinction as single base pair change missense mutations make up all *GRIN2A* patient-reported missense variants within ClinVar, suggesting that within *GRIN2A*, simultaneous double nucleotide changes are exceedingly rare. The reason behind this can be speculated through the back of a napkin calculation. With an estimated human *de novo* mutation rate of 1.2×10^{-8} per nucleotide per generation (Kong et al., 2012), a simultaneous double-nucleotide mutation rate would be 1.44×10^{-16} per nucleotide per generation. This means that if every human alive had two offspring, it would require over 1,000 generations for a double nucleotide mutation to occur within *GRIN2A*. It should be noted that this calculation makes a number of incorrect assumptions such as a constant mutation rate throughout the genome (Chuang and Li, 2004), that mutation events are independent (Averof et al., 2000) and that *de novo* mutations are the only means of acquiring a missense mutation (Yang and Rannala, 2012). Nonetheless, a lack of patient data indicating that these events produce deleterious mutations within *GRIN2A* makes it pragmatic to exclude them from studies hoping to get ahead of patient-reported variants.

In Vitro Site-Directed Mutagenesis:

Oligonucleotide primers meant to introduce the mutant into a *GRIN2A*-WT template were created and ordered using Agilent's Primer Design tool. This was performed by uploading the *GRIN2A* reference sequence (GenBank accession numbers, NM_000833.3), identifying the location of the desired mutation, and the codon change needed to confer this mutation. The Agilent Primer Design Tool produced a forward and reverse primer sequence, which was

documented and ordered. 125ng of forward and reverse primer were added to a 500 µl PCR tube along with 5 ng of dsDNA wild-type template, 5 µl of reaction buffer, 1 µl of dNTP mix, 39.5 µl of DI water and 2.5 U of DNA polymerase. Variant DNA was amplified by PCR. Upon completion of the last PCR cycle 10 U of *Dpn1*, a methylation-dependent endonuclease, was added to the PCR product to degrade the dsDNA wild-type template. The PCR product containing the *Dpn1* was then gently mixed, spun down, and incubated at 37°C for 1 hour.

Transformation

After incubation, the PCR product was either frozen at -4°C or transformed into E. coli using a heat shock method. The transformation was performed by adding 1 µl of PCR product to ~ 5 µl of XL10-Gold® ultracompetent E. coli cells in a 1.5 ml Eppendorf tube. This mixture was then incubated on ice for 15 minutes. The Eppendorf tube was then transferred to a 42°C bath for 45 seconds before being incubated on ice two more minutes. This rapid change in temperature increases the permeability of E. coli membranes to plasmid DNA. In addition, XL10-Gold® ultracompetent cells are suspended in a solution containing divalent cations such as Ca^{++}, which assist in the permeation of plasmid DNA through a process known as chemical transformation. After the 2-minute ice incubation, 500 µl of SOC media was added to the transformed cells and incubated for 37°C for 1 hour. SOC media contains several cations and chemicals which increase the efficiency of chemical transformation as well as providing a growth media for competent cell growth. After the incubation period, the cells were then spread over agar plates containing ampicillin and incubated at 37°C for 12-16 hours, after which time E. coli colonies begin to form. Visible colonies were then transferred from the agar plates to 3ml of ampicillin containing 2xYT media using an inoculation loop and were then placed in the incubated at 37°C for 12-16 hours, allowing the plasmid DNA to replicate further.

Plasmid DNA was then extracted and purified from successfully transformed E. coli using the QIAprep Miniprep Kit High-Yield Protocol from Qiagen (Valencia, CA). This process was performed by pelleting the bacterial growth and removing the liquid growth medium from each Eppendorf tube. A lytic reagent was then used to lyse the E. coli, releasing the plasmid DNA into solution. Several reagents were then used to extract and purify the plasmid DNA. A CP4 primer and a small sample of plasmid DNA were then sequenced via Eurofins MWG Operon (Huntsville, AL) to verify that the variant had been installed. After mutant installation verification, the NEO primer was used to sequence the beginning of the open reading frame to verify not second mutation had been installed into the plasmid DNA.

DNA Linearization

Variant plasmid DNA was then linearized using a Not1 restriction enzyme. Linearization is performed in order to prepare the DNA for RNA synthesis. This is necessary because *in vivo* plasmid DNA exists as a tightly wound supercoiled circle. RNA polymerase has a high processivity, meaning that it will continue to catalyze reactions without releasing from its substrate. As a consequence of this, RNA polymerase will travel around plasmid DNA multiple times and produce an RNA sequence that is longer than intended. The use of Not1 on plasmid DNA prevents this from occurring by breaking the bonds responsible for the circular geometry of plasmid DNA and creating a linear DNA strand of proper sequence length. DNA linearization was done according to manufacturer instructions (Ambion/Life Technologies, Austin, TX). DNA linearization was verified using gel electrophoresis.

RNA Synthesis

Verified linearized DNA was then used to synthesize mRNA according to manufacturer instructions using mMessage mMachine T7 kit (Ambion/Life Technologies, Austin, TX), yielding 10-30 µg of mRNA. Gel electrophoresis was used to verify mRNA production.

Two Electrode Voltage Clamp (TEVC)

Variant GluN2A mRNA was then mixed with equal parts wildtype GluN1 mRNA, and 50-100 nL of mRNA mixture containing 5-10 ng of mRNA was injected into ~25 *Xenopus laevis* oocytes obtained from Xenopus 1 Inc. using a Drummond Nanoject II (Broomall, PA). Oocytes were then incubated in Barth's solution at 18°C for 1-3 days. Barth's solution contained (in mM): 88 NaCl, 1 KCl, 24 $NaHCO_3$, 10 HEPES, 0.82 $MgSO_4$, 0.33 $Ca(NO_3)_2$, 0.91 $CaCl_2$, 100 µg/ml gentamycin, 40 µg/ml streptomycin, and 50 µg/ml penicillin. A dissecting scope facilitated the placement of two oocytes into the recording chambers of one of two perfusion tracks. Two electrode voltage clamps, Warner model OC725B (Hamden, CT), were used to create a membrane potential across the oocytes and measure changes in current occurring in response to a series of solutions containing varying concentrations of ligands. Easy Oocyte software was used to record these changes and produced a graph which looks like:

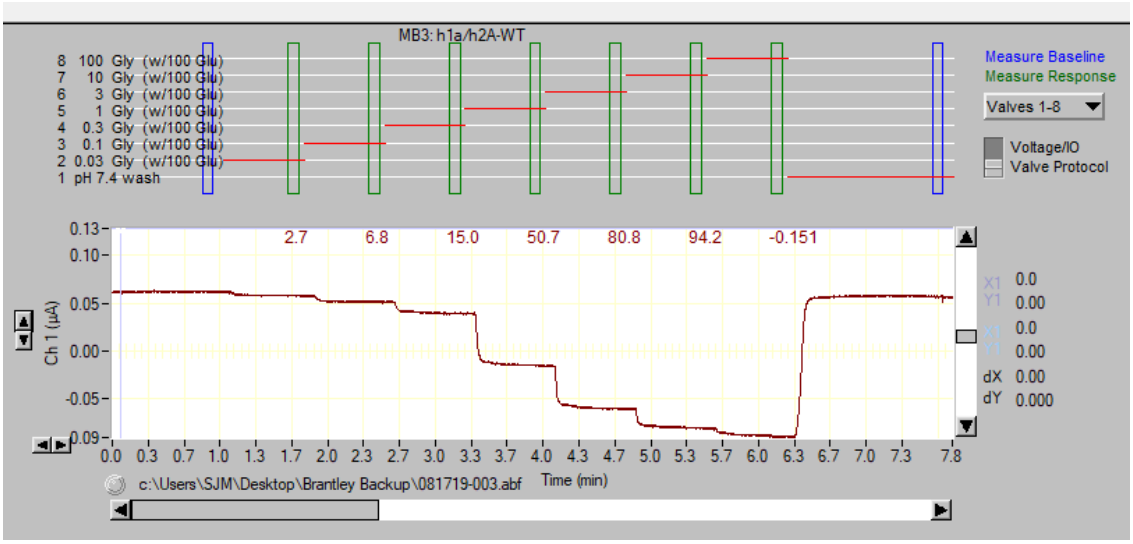

Figure 11: Wildtype GluN2A receptor during a 7-concentration glycine assay. This graph produced by Easy Oocyte during a TEVC experiment. Negative reference currents are reported for positive currents flowing through NMDA receptors and the numbers are reported in red at the top of the graph represented percent of current present at that time in reference to the final maximal current which is not reported by Easy Oocyte and normalized to 100%.

Agonists Assays:

A 7-concentration glutamate assay was performed by titrating wash solution containing seven concentrations: 0.1, 0.3, 1, 3, 10, 30, and 100 µM of glutamate and 100 µM of glycine. The wash solution contained (in mM): 90 NaCl, 1 KCl, 10 HEPES, 0.5 BaCl2, 0.01 EDTA, at pH 7.4. This was to obtain the receptor's glutamate log[EC_{50}]. This value represents the log[agonist] required to reach 50% of the maximal excitatory response. A 7-concentration glycine assay was performed by titrating wash solution containing 0.3, 0.1, 0.3, 1, 3, 10, and 100 µM of glycine and 100 µM of glutamate. This was to obtain the receptor's glycine log[EC_{50}]. The oocytes were then held at -40 mV during this assay.

Negative Allosteric Modulator Assays:

A 7-concentration Zinc assay was performed by titrating wash solution containing seven concentrations: 1, 3, 10, 30, 100, and 300 nM of Zinc along with 50 µM of glutamate and 50 µM of glycine. The wash solution contained (in mM) 90 NaCl, 1 KCl, 10 HEPES, 10 tricine and 1.0 $BaCl_2$, pH 7.3. The tricine buffer was used to maintain proper Zn^{++} concentration. The oocytes were held at -20 mV. This was to obtain the receptors log[IC_{50}] as well as the % of residual current present at 300 nM of Zinc.

A single concentration H^+ inhibition assay was performed by using the same wash solution as the agonist assays with 100 µM of glutamate and glycine. The solution was then changed to 7.6 pH through the addition of 6 N NaOH. This solution was then aliquoted into two containers, and one of the solutions was changed to 6.8 pH. The difference in activation between the two solutions was then reported as a percentage.

pOPEN Assay:

An assay used to calculate the P_{OPEN}, a measure of the time a single ion channel remains open over a given period of time, was then performed using methanethiosulfonate-ethyl ammonium (MTSEA), a compound that opens NMDA receptors containing a GluN1-A652C subunit. This was done using the same wash solution as the agonists at pH 7.4, 100 µM of glutamate and glycine, and 10mM MTSEA. Wash solution was perfused over the oocytes for 30 seconds before the wash solution containing 100 µM of glutamate and glycine was perfused for another 30 seconds. After 1 minute, the solution containing 200 µM of MTSEA was perfused over the oocytes for 3 minutes. This gave the percentage difference of receptor current in the

solution containing just the agonist and then the solution containing MTSEA. Receptor P_{OPEN} was then calculated using this equation:

$$pOPEN = \frac{(100 * 44)}{(\%\ potentiation * 66)}$$

This assay is made possible by the amino acid change in the GluN1 subunit. MTSEA acts as a cysteine modulator and when receptor channels are opened agonist and co-agonist binding the MTSEA covalently binds to cysteine residues in the M3 domain of the GluN1 subunit, inducing conformational changes which lock the receptor in an open position, increasing its efficacy to 1.0 (Chang and Kuo, 2008; Yuan et al., 2009). This was performed at -40mV and is reported as a percentage.

Results:

Calculation/Reporting:

Two-electrode voltage-clamp oocyte recordings were performed on GluN1-WT/GluN2A-WT and on GluN1-WT/GluN2A-variant receptors. Each assay was performed on 10-12 oocytes per variant, across two injection cycles averaging around six oocyte recordings per variant, per injection cycle. Glutamate log[EC_{50}], Glycine log[EC_{50}], and Zinc log[IC_{50}] were generated using GraphPad Prism 8 along with dosage response curves similar to (Graph 1-3). Wildtype NMDA receptors were used as a control, and six oocytes were recorded at the beginning of every new assay. These GluN1-WT/GluN2A-WT controls were performed for each assay, and this data was aggregated based on the amino acid residue to create a multiday control value. Statistical significance was established by comparing overlap in this multiday control 95% CI and with a 95% confidence interval calculated from variant obtained data points. All statistical analysis was performed on the experimentally derived data points. The log[EC_{50}/ IC_{50}] values were then converted into molar concentrations and reported in Table 1-14 along with SEM and n-values.

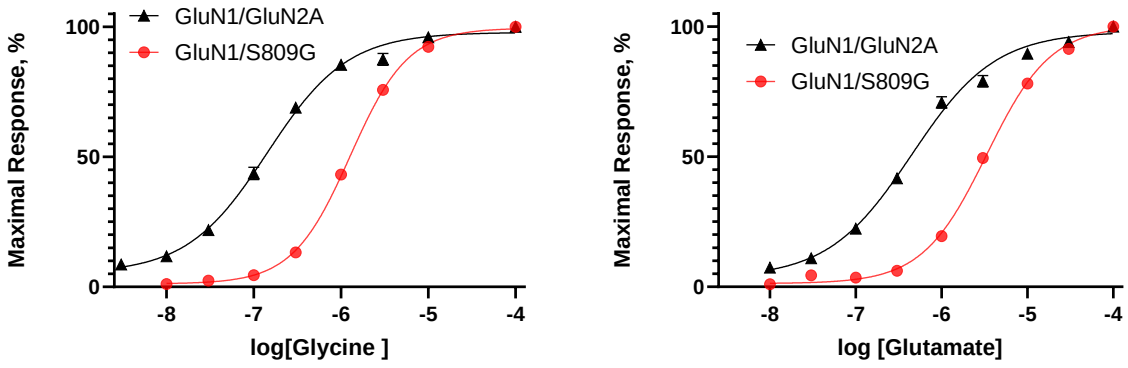

Figure 12 Agonist concentration-effect curves for variant GluN2A-S809G.

Agonists log[EC_{50}] values were calculated using this equation:

$$Y = \text{Bottom} + \frac{(\text{Top} - \text{Bottom})}{1 + 10\text{^}((\log[\text{EC50}] - \text{X}) \times \text{HillSlope}))}$$

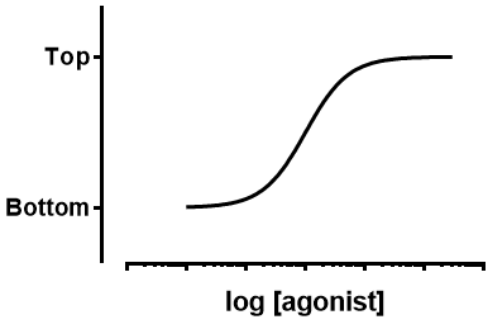

Figure 13 Hypothetical agonist concentration effect curve

where Bottom represents the smallest extrapolated value of excitation, and Top is the highest degree of activation, which was normalized to 100%. Hillslope is a unitless coefficient used to describe the slope of the dosage response curve (Figure 12). The top values are normalized to 100% activation. 95% confidence interval of log[EC_{50}] was calculated by GraphPad during this analysis.

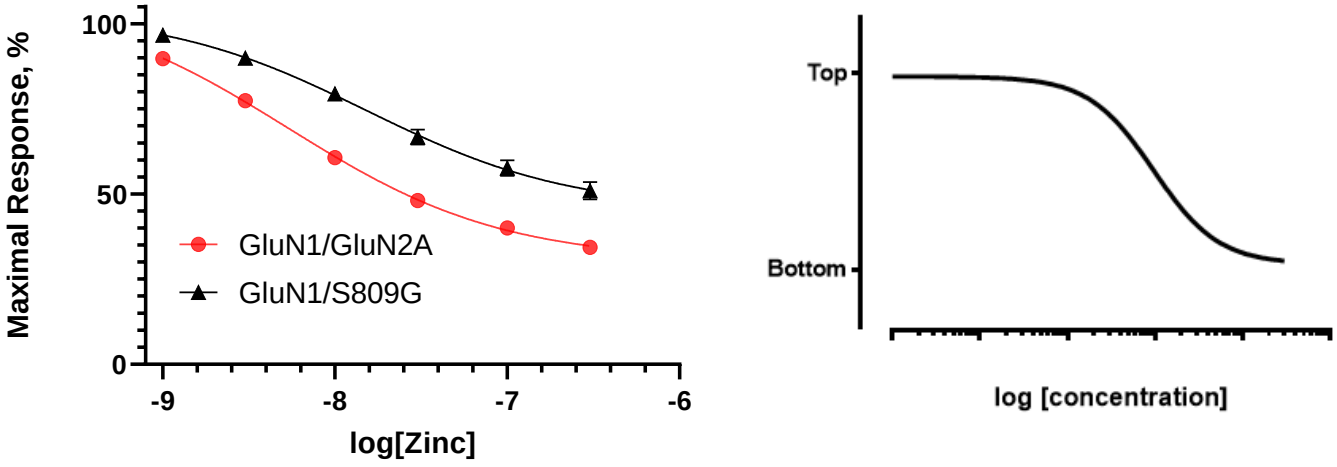

Figure 14 Inhibitor concentration-effect curve for variant GluN2A-S809G beside a hypothetical inhibitor concentration-effect curve

The potency of negative allosteric modulators was gathered through a similar means. Inhibition through chelatable was calculated similarly to log[EC_{50}], by using this equation:

$$Y = \text{Bottom} + \frac{(\text{Top} - \text{Bottom})}{(1 + 10\text{^}((\text{LogIC50} - \text{X}) \times \text{HillSlope}))}$$

where Top and Bottom correspond to the regions displayed in figure 14, and hillslope is a unitless coefficient used to describe the slope of the dosage response curve. The top value is standardized to 100, and the bottom value is not restricted. The bottom value is reported as Zinc y-min, a description of the residual current left at max 300nM Zinc concentration. The overlap between variant log[IC_{50}] 95% CI's and multiday wildtype control 95% CI's were used to establish statistical significance. Proton inhibition is reported as a Current Response, % (IpH6.8/IpH7.6,%), a single percentage.

Data Collection/Experimental Constraints:

Of the 42 variants initially calculated, four had been reported in patients previous to the variant determination process, and functional data on these variants were available. These variants were: GluN2A-S809R, -L812Q, -M817R, and -A818T. This variant information is reported in the pharmacology tables alongside functional data obtained through this project. Functional data were available on other missense variants occurring in this region that were not determined during this process. These variants are GluN2A-L812M and -V820G. Their functional data is also reported in the pharmacology tables. In addition, data was not able to be collected on three variants due to experimental constraints. These variants are GluN2A-Q811L, -N816D, -M817R, and -G819D. No data is reported on these variants, and they are not included in the pharmacology tables.

Variant Population Data:

GRIN2A has a robust clinical population, with 287 patient-reported missense mutations. Within the reported missense mutations, 17 are classified as pathogenic, 26 as likely pathogenic, 184 as uncertain significance, 23 likely benign, and 0 are classified as benign. Another 24 have conflicting interpretations and are not classified. Within amino acids 808-821 there are 8 missense variants reported:

Allele Reference	Variant	Classification	n-value
486724	h2A-A818E	Likely pathogenic	n=2
522855	h2A-A818T	Conflicting interpretations	n=2
803217	h2A-M817T	Likely Pathogenic	n=1
423745	h2A-M817R	pathogenic	n=1
205659	h2A-M817V	pathogenic	n=1
570650	h2A-D815E	Uncertain significance	n=1
401964	h2A-I814T	Likely benign	n=1
409817	h2A-S809R	Likely pathogenic	n=1

The presence of variants at previously verified pathogenic and likely pathogenic amino acids s considered strong evidence of pathogenicity. All variants at amino acid residues h2A-S809, -M817, and A818E have a (PS1) line of evidence for pathogenicity.

Control population data was then collected from gnomAD v2.1.1 and gnomAD v3.1.

Allele Number	Variant	Allele Frequency
143294	h2A-G819S	6.98e-6
251186	h2A-A818V	3.98e-6

While both variants have unusually small allele frequencies, their presence in the control population will be considered when interpreting their significance. No variants allelic frequency was significantly higher than in either control or affected populations. In addition, these variants occur in a region with low reports of benign variants (PP2).

Variant Type and Loci:

All of these variants were created through missense mutations, and no stop codons were created through these mutations meaning that the length of the gene product was unaffected by these mutations. According to this region's MTR values and along with the fact that it is enriched with patient-reported mutations, these amino acids can be considered to be in a mutational hot spot (PM1).

Clinical Data:

No clinical data is available for these variants, as none of them have been reported in patients. From the clinical reports of variants in this region, it is likely that patients would present with an epilepsy-aphasia disorder with the possibility of developmental delay. Other clinically obtainable data include mode of inheritance, family history, or co-segregation of disease. Due to these restraints, the following ACMG lines of evidence are unavailable: (PS2, PP1, PM3, PP4, and BP2, BS2). While no familial history is available to us, those variants without any lack of

genetic data can be assumed to occur due to a *de novo* mutation. The lack of familial genetic data prevents us from knowing this (PS2), but it can be assumed (PM6); thus, all variants with n-values of 0 are assumed to be *de novo.*

Functional Analysis:

The ACMG states that well-established functional studies finding support that a mutation has damaging effects on a gene product are strong evidence for pathogenicity (PS3). There are no guidelines provided by the ACMG or any other institution which define what changes in pharmacological profiles of NMDARs should be considered pathogenic. It is well established that changes in the pharmacological profiles of NMDARs can cause them to be disease-causing though the exact threshold of what magnitude of change *can* result in a pathogenic variant or even what magnitude of change *does* result in pathogenic phenotypes remains unknown. By making observations from clinically reported variants in this region, the range of perturbation of agonist binding potency is from 1.5 to >20 fold. Changes in allosteric modulators ranged from 1.5 to 3-fold for H^+ and 1.1 to 3.5-fold shift for Zinc potency. From these observations, I decided that any variant which had 3 statistically significant shifts whose fold variance summed to be greater than 4 would be considered a damaging effect. If a variant has a single fold change in any of the assays conducted, which was greater than 3-fold, then this variant would be considered damaging. If any variant which had a shift in ≥4 in any of the assays conducted, then this would be considered damaging. Lastly, if not statistically significant shifts were observed at all, then it was considered evidence that the variant was benign according to BP3.

In-silico Modeling

No *in-silico* modeling was performed to analyze these variants, and therefore no predictions were made based on these models. From this, ACMG guidelines PP3 and BP4 were not used.

Classification of using ACMG standards and guidelines for the interpretation of sequence variants:

Variants evidence was classified using evidence from figure 16, and criteria was condensed using rules outlined in figure 15.

Variant	Effect	Evidence
h2A-M808V	Pathogenic (IIIa)	PS3, PM1, PM2, PM6
h2A-M808I	Pathogenic (IIIa)	PM1, PM2, PM6, PS3
h2A-M808L	Pathogenic (IIIa)	PM1, PM2, PM6, PS3
h2A-S809G	Pathogenic (IIIa)	PM1, PM2, PM5, PM6, PS3
h2A-S809C	Likely pathogenic (IV)	PM1, PM2, PM5, PM6
h2A-S809R	Pathogenic (IIIa)	PM1, PM2, PM5, PM6, PS3
h2A-S810R	Pathogenic (IIIa)	PS3, PM1, PM2, PM6
h2A-S810G	Likely pathogenic (IV)	PM1, PM2, PM6
h2A-S810N	Likely pathogenic (IV)	PM1, PM2, PM6
h2A-Q811H	Likely pathogenic (IV)	PM1, PM2, PM6
h2A-Q811R	Pathogenic (IIIa)	PM1, PM2, PM6, PS3
h2A-L812V	Pathogenic (IIIa)	PS3, PM6, PM5, PM2, PM1
h2A-L812R	Pathogenic (IIIa)	PM1, PM2, PM5, PM6, PS3
h2A-L812M	Pathogenic (IIIa)	PS3, PM1, PM2, PM5, PM6
h2A-D813N	Pathogenic (IIIa)	PM1, PM2, PM6, PS3
h2A-D813Y	Pathogenic (IIIa)	PS3, PM1, PM2, PM6
h2A-D813E	Pathogenic (IIIa)	PS3, PM1, PM2, PM6
h2A-I814F	Pathogenic (IIIa)	PS3, PM1, PM2, PM6
h2A-I814N	Likely pathogenic (IV)	PM1, PM2, PM6
h2A-I814S	Pathogenic (IIIa)	PS3, PM1, PM2, PM6

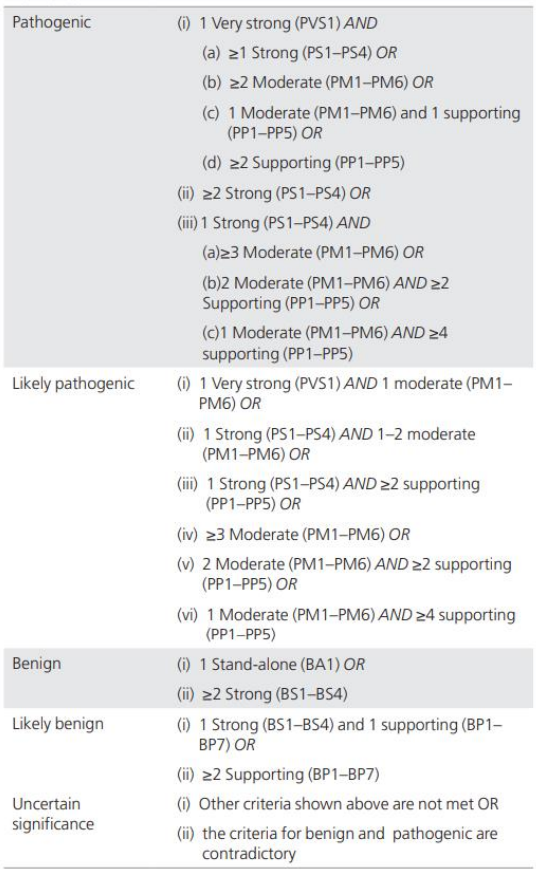

Pathogenic	(i) 1 Very strong (PVS1) *AND* (a) ≥1 Strong (PS1–PS4) *OR* (b) ≥2 Moderate (PM1–PM6) *OR* (c) 1 Moderate (PM1–PM6) and 1 supporting (PP1–PP5) *OR* (d) ≥2 Supporting (PP1–PP5) (ii) ≥2 Strong (PS1–PS4) *OR* (iii) 1 Strong (PS1–PS4) *AND* (a)≥3 Moderate (PM1–PM6) *OR* (b)2 Moderate (PM1–PM6) *AND* ≥2 Supporting (PP1–PP5) *OR* (c)1 Moderate (PM1–PM6) *AND* ≥4 supporting (PP1–PP5)
Likely pathogenic	(i) 1 Very strong (PVS1) *AND* 1 moderate (PM1–PM6) *OR* (ii) 1 Strong (PS1–PS4) *AND* 1–2 moderate (PM1–PM6) *OR* (iii) 1 Strong (PS1–PS4) *AND* ≥2 supporting (PP1–PP5) *OR* (iv) ≥3 Moderate (PM1–PM6) *OR* (v) 2 Moderate (PM1–PM6) *AND* ≥2 supporting (PP1–PP5) *OR* (vi) 1 Moderate (PM1–PM6) *AND* ≥4 supporting (PP1–PP5)
Benign	(i) 1 Stand-alone (BA1) *OR* (ii) ≥2 Strong (BS1–BS4)
Likely benign	(i) 1 Strong (BS1–BS4) and 1 supporting (BP1–BP7) *OR* (ii) ≥2 Supporting (BP1–BP7)
Uncertain significance	(i) Other criteria shown above are not met OR (ii) the criteria for benign and pathogenic are contradictory

Figure 15 Rules for condensing ACMG lines of evidence ((Courtesy Richard et al., 2015)

h2A-D815H	Pathogenic (IIIa)	PS3, PM1, PM2, PM6
h2A-D815Y	Pathogenic (IIIa)	PS3, PM1, PM2, PM6
h2A-D815H	Likely pathogenic (IV)	PM1, PM2, PM6
h2A-N816T	Pathogenic (IIIa)	PS3, PM1, PM2, PM6
h2A-N816K	Pathogenic (IIIa)	PS3, PM1, PM2, PM6
h2A-A818V	Likely pathogenic (II)	PS3, PM1
h2A-A818P	Pathogenic (IIIa)	PS3, PM1, PM2, PM6
h2A-G819C	Pathogenic (IIIa)	PM1, PS3, PM2, PM6
h2A-G819S	VUS - not enough evidence	PM1
h2A-V820A	VUS - not enough evidence	BS3, PM2, PM6
h2A-V820E	Pathogenic (IIIa)	PS3, PM1, PM2, PM6
h2A-F812L	Likely pathogenic (IV)	PM1, PM2, PM6
h2A-F821C	Pathogenic (IIIa)	PM1, PS3, PM2, PM6
h2A-F821I	Pathogenic (IIIa)	PS3, PM1, PM2, PM6

Evidence of pathogenicity	Category
Very strong	PVS1 null variant (nonsense, frameshift, canonical ±1 or 2 splice sites, initiation codon, single or multiexon deletion) in a gene where LOF is a known mechanism of disease Caveats: • Beware of genes where LOF is not a known disease mechanism (e.g., *GFAP*, *MYH7*) • Use caution interpreting LOF variants at the extreme 3′ end of a gene • Use caution with splice variants that are predicted to lead to exon skipping but leave the remainder of the protein intact • Use caution in the presence of multiple transcripts
Strong	PS1 Same amino acid change as a previously established pathogenic variant regardless of nucleotide change Example: Val→Leu caused by either G>C or G>T in the same codon Caveat: Beware of changes that impact splicing rather than at the amino acid/protein level PS2 De novo (both maternity and paternity confirmed) in a patient with the disease and no family history Note: Confirmation of paternity only is insufficient. Egg donation, surrogate motherhood, errors in embryo transfer, and so on, can contribute to nonmaternity. PS3 Well-established in vitro or in vivo functional studies supportive of a damaging effect on the gene or gene product Note: Functional studies that have been validated and shown to be reproducible and robust in a clinical diagnostic laboratory setting are considered the most well established. PS4 The prevalence of the variant in affected individuals is significantly increased compared with the prevalence in controls Note 1: Relative risk or OR, as obtained from case–control studies, is >5.0, and the confidence interval around the estimate of relative risk or OR does not include 1.0. See the article for detailed guidance. Note 2: In instances of very rare variants where case–control studies may not reach statistical significance, the prior observation of the variant in multiple unrelated patients with the same phenotype, and its absence in controls, may be used as moderate level of evidence.
Moderate	PM1 Located in a mutational hot spot and/or critical and well-established functional domain (e.g., active site of an enzyme) without benign variation PM2 Absent from controls (or at extremely low frequency if recessive) (**Table 6**) in Exome Sequencing Project, 1000 Genomes Project, or Exome Aggregation Consortium Caveat: Population data for insertions/deletions may be poorly called by next-generation sequencing. PM3 For recessive disorders, detected in *trans* with a pathogenic variant Note: This requires testing of parents (or offspring) to determine phase. PM4 Protein length changes as a result of in-frame deletions/insertions in a nonrepeat region or stop-loss variants PM5 Novel missense change at an amino acid residue where a different missense change determined to be pathogenic has been seen before Example: Arg156His is pathogenic; now you observe Arg156Cys Caveat: Beware of changes that impact splicing rather than at the amino acid/protein level. PM6 Assumed de novo, but without confirmation of paternity and maternity
Supporting	PP1 Cosegregation with disease in multiple affected family members in a gene definitively known to cause the disease Note: May be used as stronger evidence with increasing segregation data PP2 Missense variant in a gene that has a low rate of benign missense variation and in which missense variants are a common mechanism of disease PP3 Multiple lines of computational evidence support a deleterious effect on the gene or gene product (conservation, evolutionary, splicing impact, etc.) Caveat: Because many in silico algorithms use the same or very similar input for their predictions, each algorithm should not be counted as an independent criterion. PP3 can be used only once in any evaluation of a variant. PP4 Patient's phenotype or family history is highly specific for a disease with a single genetic etiology PP5 Reputable source recently reports variant as pathogenic, but the evidence is not available to the laboratory to perform an independent evaluation

LOF, loss of function; OR, odds ratio.

Figure 16: Specific lines of evidence for variant interpretation provided by the ACMG (Courtesy: Richards et al., 2015)

Functional Analysis:

Pre-M4 (AA 808-816) Mutations Enhance Agonist Potency

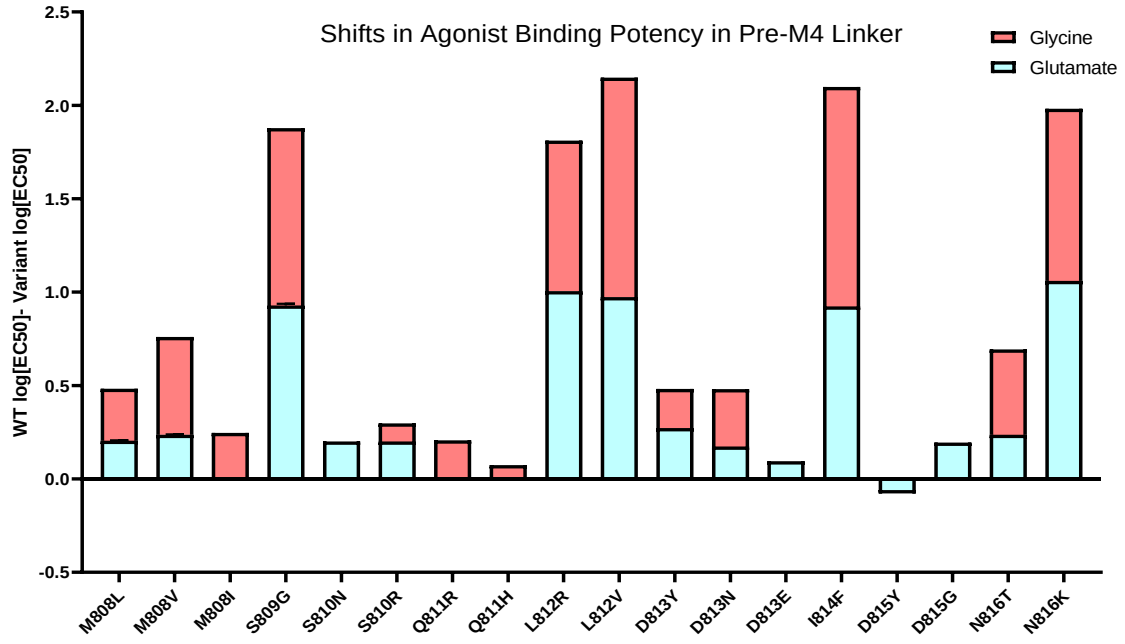

Figure 17: Statistically significant agonist binding potency of variants in the pre-M4 linker are displayed. Agonist binding potency is displayed as the difference between WT log[EC_{50}] and Variant log [EC_{50}]. Positive values represent an increase in agonist binding potency and negative values represent a decrease in agonist binding potency.

Of the 23 variants tested reported within the pre-M4 linker, 14 resulted in an increase in glutamate potency, and only one resulted in a decrease in glutamate potency, h2A-D815Y. 11 out of the 24 variants tested exhibited an increase in glycine potency with no decreases in glycine potency reported for variants within this region. Changes in agonist potency frequently cooccurred with exactly half, 12 variants, displaying a shift in both glutamate and glycine potency. All agonist binding potency shifts were consistent and occurred in the same direction. Every amino acid residue had at least one variant, which increased agonist binding potency.

M4 (AA 817-821) Mutations Enhance Agonist Potency

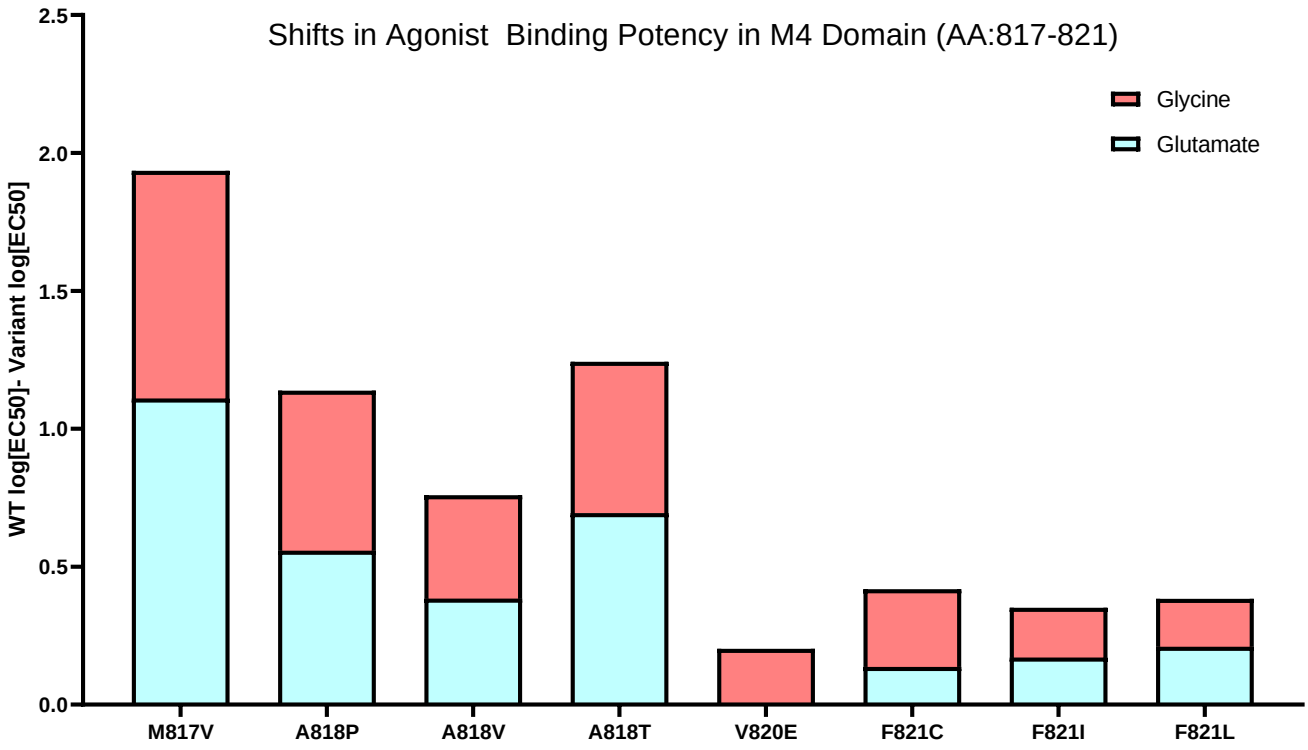

Figure 18: Figure 17: Statistically significant agonist binding potency of variants in the M4 domain are displayed. Agonist binding potency is displayed as the difference between WT log[EC_{50}] and Variant log [EC_{50}]. Positive values represent an increase in agonist binding potency and negative values represent a decrease in agonist binding potency.

Agonist binding potency was affected by mutations occurring within the M4 domain. These changes occurred in a similar manner to the shifts observed in the pre-M4 linker. Of the 11 variants tested, 8 resulted in statistically significant gain-of-function shifts. Of which all but one variant displayed statistically significant shifts in both glutamate and glycine potency. No G819 variant resulted in a change in agonist potency.

Pre-M4 (AA 808-816) Mutations Result in Changes to H^+ Inhibition

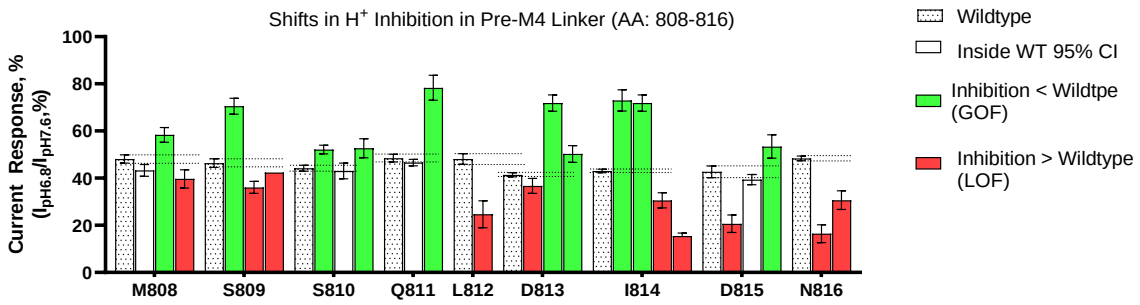

Figure 19: Variant proton inhibition is presented for variants in the pre-M4 linker. Proton inhibition is presented as the current response, % in wash solution of pH 6.8 versus pH 7.6. The dotted bars represent the wildtype proton inhibition, green shaded bars represent gain of function variants, red shaded bars represent loss of function variants and white shaded bars represent variants whose 95% CI overlapped with the WT 95% CI. The dotted lines represent the multiday control 95% CI and the error bars represent each variant's 95% CI.

Of the 23 variants in the pre-M4 linker tested for H^+- inhibition, 19 had statistically significant shifts in the degree to which increased H^+ concentration inhibited function. 12 of these changes resulted in a loss of inhibition or a gain-of receptor function. The other 7 variants had an increase in inhibition in the presence of increased H^+ concentration, resulting in a loss-of-receptor function. Every amino acid had at least one variant which exhibited a change in H^+ inhibition.

M4 (AA 817-821) Mutations Result in Changes to H^+ Inhibition

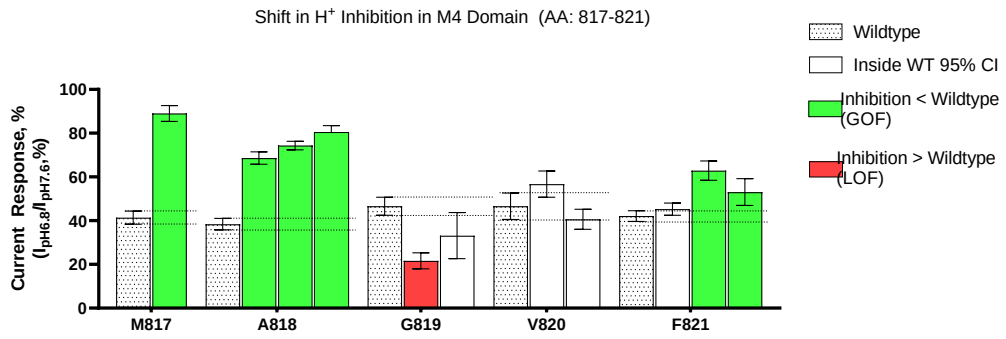

Figure 20: Variant proton inhibition is presented for variants in the M4 domain. Proton inhibition is presented as the current response, % in wash solution of pH 6.8 versus pH 7.6 solution. The dotted bars represent the wildtype proton inhibition, green shaded bars represent gain of function variants, red shaded bars represent loss of function variants and white shaded bars represent variants whose 95% CI overlapped with the WT 95% CI. The dotted lines represent the multiday control 95% CI and the error bars represent each variant's 95% CI.

Of the 11 variants in the M4 domain tested for H^+ inhibition, 7 had statistically significant shifts in the degree to which H^+ inhibited function. 6 of these changes resulted in a loss of inhibition or a gain-of receptor function. While only 1 (GluN2A-G819S) variant had an increase in inhibition in the presence of increased H^+ concentration, resulting in a loss-of receptor function. No V820 variants resulted in a shift in H^+ inhibited. The dotted lines represent the multiday control 95% CI.

Pre-M4 (AA 808-814) Mutations Result in Changes to Zn^{++} Inhibition Potency and Maximal Zn^{++} Inhibition

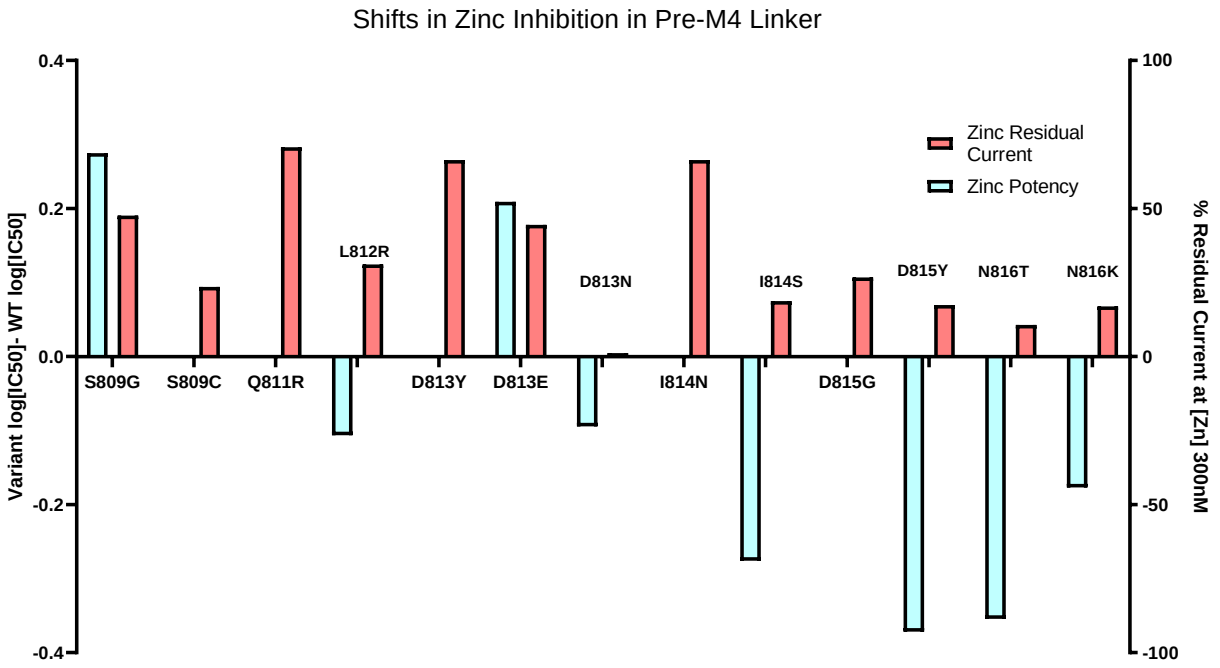

Figure 21: Statistically significant zinc binding potency for variants in the pre-M4 linker are displayed in blue as the difference between variant log[IC_{50}] and WT log[IC_{50}]. Positive values represent a decrease in zinc binding potency and negative values represent an increase in zinc binding potency. Statistically significant % residual current at 300 nM of zinc is displayed in red for pre-M4 variants.

Of the 23 variants in the pre-M4 linker tested for Zn^{++} inhibition, 12 had statistically significant shifts in Zn^{++} potency. All of these resulted in a loss of inhibition or a gain of receptor function. Of the 23 variants tested, 8 had a statistically significant change in the maximum inhibition observed by 300nM of Zinc. These changes were not as consistent as the change in Zn^{++} potency with 2 resulting in a decreased maximum inhibition and 4 resulting in an increase in the ability of Zn^{++} to inhibit receptor function. Changes in Zinc potency and maximal inhibition did not necessarily occur together, with three variants displaying a change in only 1 of these criteria.

M4 (AA 817-821) Mutations Result in Changes to Zn^{++} Inhibition Potency and Maximal Zn^{++} Inhibition

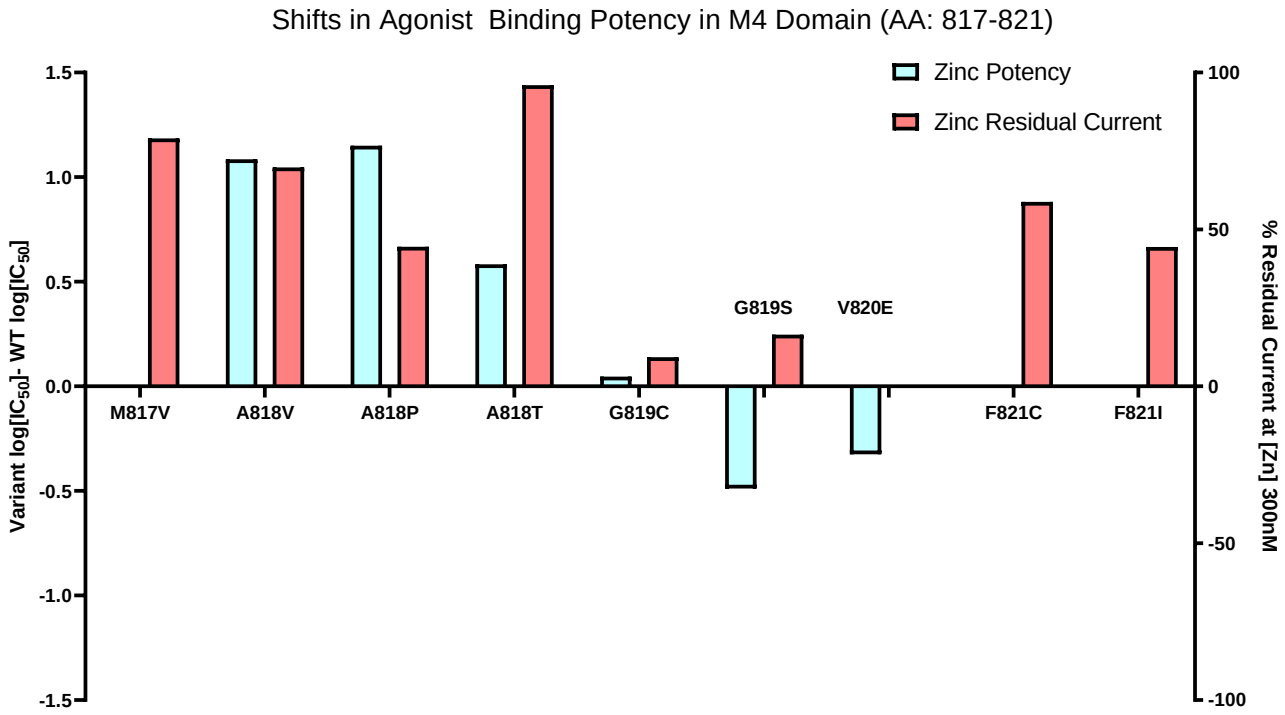

Figure 22: Statistically significant zinc binding potency for variants in the M4 domain are displayed in blue as the difference between variant log[IC_{50}] and WT log[IC_{50}]. Positive values represent a decrease in zinc binding potency and negative values represent an increase in zinc binding potency. Statistically significant % residual current at 300 nM of zinc is displayed in red for M4 domain variants.

Of the 11 variants in the M4 domain tested for Zn^{++} inhibition, 8 had statistically significant shifts in Zn^{++} potency. All of these resulted in a loss of inhibition or a gain of receptor function. Of the 11 variants tested, 6 had a statistically significant change in the maximum inhibition observed by 300nM of Zinc. These changes were not as consistent as the change in Zn^{++} potency with 4 resulting in a decreased maximum inhibition and 2 resulting in an increase in the ability for of Zn^{++} to inhibit receptor function. Changes in Zinc potency and maximal inhibition did not necessarily occur together, with 4 variants displaying a change in only 1 of these criteria.

Missense Mutations Result in Varied and Dramatic Changes to Receptor P_{OPEN}

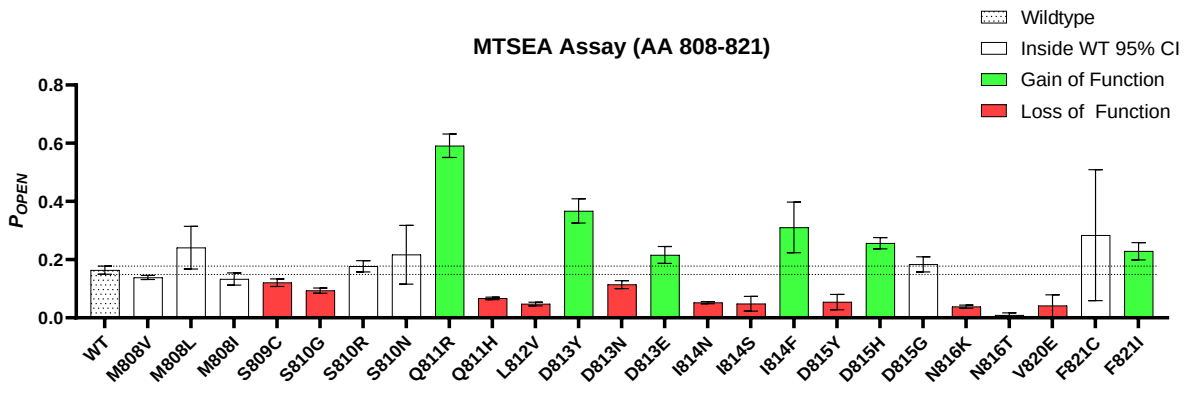

Figure 23: All variant P_{OPEN} data is displayed here. The dotted bars represent the wildtype P_{OPEN}, green shaded bars represent gain of function variants, red shaded bars represent loss of function variants and white shaded bars represent variants whose 95% CI overlapped with the WT 95% CI. The dotted lines represent the multiday control 95% CI and the error bars represent each variant's 95% CI.

Of the 24 variants with the AA sequence 808-821 whose open probability was analyzed, 17 resulted in a statistically significant change in receptor P_{OPEN}, of which 6 resulted in a larger P_{OPEN} while the other 11 presented as loss of function. This is in contrast to other assay results where receptor function was enhanced more than it was dampened. The dotted lines represent the multiday control 95% CI.

Discussion:

Missense mutations in amino acid residues 808-821 of the *GRIN2A* gene resulted in large scale and definable changes to key receptor functions. The most extreme and consistent change observed increased agonist binding potency, where all but seven variants exhibited shifts in agonist potency. When an increase in glutamate binding potency was observed, it frequently co-occurred with changes in glycine potency, and these shifts occurred in similar magnitudes. These changes to agonist binding potency are consistent with previously described variant functions of this region as well as clinical presentations of patient's with pathogenic variants in this region.

Changes in the potency of negative allosteric modulators Zn^{++} and H^{+} were also observed in all but three variants, h2A-Q811H, -V820E, and -D815H. These changes resulted in both increased and decreased degrees of inhibition. In addition, the effect size of these modulators was changed. In the oocyte model, these changes resulted in definable gain of function or loss of function receptors. These changes may display differently *in vivo* due to differences in the molecular and chemical environments of oocytes versus those of native neurons. Decreases in negative allosteric modulator potency or effect size may not necessarily result in over-active neural circuits in the same way changes in agonist potency may. It is also not known whether changes in maximum inhibition or in modulator potency are more important in the development of neuropathologies. Further evaluation of the states at which native NMDARs exist will be important in determining the significance of these factors, though such evaluation has proven to be difficult. For example, reports of synaptic Zn^{++} concentration range from 10nM to >100 μM (Auton et al., 2015; Zhang et al., 2016), meaning that native NMDARs could be inhibited to anywhere ranging from 75-40% under normal physiological conditions. If a mutation were to affect Zinc maximal inhibition properties, this could offset the effects of slight changes in

agonist potency and become the dominating effect on receptor function, though to what degree or if this occurs remains unknown. The synaptic concentration of free Zinc is difficult to characterize due to experimental constraints, preventing a full translation of this work into *in vivo* understanding.

Lastly, changes in P_{OPEN} were large and varied. Changes in receptor P_{OPEN} were not as prevalent as changes in agonist potency and allosteric modulator potency; however, their effect size was large and unpredictable. There was no clear pattern to the magnitude or direction of change within a receptor region or amino acid residue. In addition, many of these changes suggest large inhibitory effects on receptor behavior, a deviation from agonist potency effects.

The pharmacological changes observed are definable as loss-of-function or gain-of-function changes within the oocyte model; however, their effects *in vivo* are less clearly defined. Increases in agonist binding potency result in increased NMDA receptor activity, which is thought to be the pathomechanisms underlying epilepsy displayed in patients with *GRIN2A*-associated pathologies. However, changes in negative allosteric modulator potency and P_{OPEN} are more difficult to relate to specific pathomechanisms. Ultimately the resultant change in neuronal excitability cannot be known from these assays alone. Determining this value requires a deeper analysis of receptor function through methods which are more costly and time intensive than TEVC. Such an evaluation could reveal more nuanced perturbations caused by these missense mutations.

Genetic information is currently being produced quicker than researchers can analyze it. In fact, it is being produced at a rate that exceeds their ability to even organize and catalog it correctly (Hamosh et al., 2000; Williams and Weng, 2019). Currently, the only means of accurately interpreting novel variants is through the use of functional analysis. However, the

large quantities of genomic data create a real need to break free from the reliance on functional evaluation for the interpretation of novel variants. Examining possible mechanisms to facilitate that movement was the ultimate goal of this thesis. Further calls for conservative experimental design are necessary. The work presented here represents a thorough evaluation of receptor function, but more reduced functional evaluations used only to understand the effect mutations have in only terms of their pathogenicity are currently under analysis and worthy of consideration (Glazer et al., 2019).

Tools such as the MTR show that non-native amino acid residues are deleterious to the GluN2A subunit function; however, the poor resolution prevents these tools from answering more nuanced questions about the importance of the native amino acid sequence. For instance, is the function of these amino acid residues fine-tuned such that any substitution will result in a pathogenic phenotype? Or is it possible that their function is not critical, but their proximity to other important residues makes the substitution of large or charged residues disruptive to functional behavior? These are answers which cannot be answered through protein modeling or diagnostic tools reliant on genomic data such as MTR but once answered can provide ways of reducing the work involved in classifying novel variants. The percentage of pathogenic variants whose pathogenicity results from changes in critical amino acids or are resultant from changes to specifically deleterious amino acids is unknown, preventing such fruitful discussion beyond mutational scans of critical regions such as this one.

Through this evaluation, four possibly critical native amino acid residues have been identified, h2A-M808, -L812, -D813, and -N816. This determination was able to be made because every variant occurring at these residues was classified as pathogenic according to the ACMG guidelines. From these results, further analysis of all variants resulting from single

nucleotide missense mutations at these four locations would be prudent in deciding for the whether three malfunctioning variants is enough to decide a residue is critical. The identification of critical native amino acid residues is helpful in reducing the workload needed when assessing variants occurring at that amino acid residue. Ultimately, this project was able to classify 32 variants previously classified as either pathogenic or likely pathogenic, a determination which was not possible in the absence of the functional data created through this research. These were results are consistent with predictions made by the MTR, reaffirming the usefulness and need for variant diagnostic tools which are defined in terms of mutation type.

This research was able to classify a large number of never reported variants and possibly identify critical native amino acids occurring within a critical region of the *GRIN2A* gene. What degree of certainty about variant pathogenicity clinicians and genetic counselors feel is enough to make clinically relevant determinations of novel variants is beyond the scope of this thesis, however, in order to make perfect determinants, novel variants require robust functional evaluation in through more thorough means provided by TEVC, even in light of the work done here. Despite the lack of resolution brought by the conclusions made here, the importance of this type of work is difficult to overstate. Mutations within *GRIN2A* affect far more than just NMDA receptor function, and the disease states resultant from these mutations are not ones of NMDA receptors, but of the entire glutamate system as a whole. Genetic disorders currently have no cure and there are no prudent means of reducing their frequently, meaning that they will continue to be an disorders that clinicians will have to treat. While no changes to patient treatment are made from the interpretation of patient-reported variants, proper diagnosis of patient afflictions remains a goal fundamental to the mission of medicine, and it is the hope of this thesis that the work presented here helps in that larger effort.

Pharmacological Data Tables:

The data is expressed as mean ± S.E.M. (*n*); *n* is the number of oocytes.

(*n*)* indicates statistical significance

Highlighted variants indicate they had historical functional data and that there data was not collected during the course of this project

Table 1

Assay	WT 2A	M808V	M808L	M808I
Glutamate, $EC_{50,}$ µM (*n*)	3.25 ± 0.21 (31)	1.7 ± 0.12 (11)*	2.08 ± 0.19 (12)*	2.84 ± 0.17 (13)
Glycine, $EC_{50,}$ µM (*n*)	1.19 ± 0.047 (35)	0.341 ± 0.041 (10)*	0.705 ± 0.068 (12)*	0.724 ± 0.056 (10)*
Proton, % (*n*)	48.1 ± 0.85 (30)	43.3 ± 1.1 (12)	58.4 ± 1.4 (11)*	40.0 ± 1.8 (11)*
Zinc, $IC_{50,}$ nM (*n*)	5.4 ± 0.43 (23)	7.6 ± 1.1 (12)	9.8 ± 2.2 (12)	4.90 ± 0.52 (12)
% Inhibited by zinc (*n*)	32.4 ± 1.4 (37)	27.2 ± 1.7 (12)	30.2 ± 3.1 (12)	39.7 ± 3.5 (12)
Calculated P_{OPEN} (*n*)	0.164 ± .044 (41)	0.138 ± .002 (3)*	0.241 ± .032 (9)*	0.1332 ± .00081 (6)*

Table 2

Assay	WT 2A	S809G	S809C	S809R
Glutamate, $EC_{50,}$ µM (*n*)	3.371 ± 0.140 (36)	0.447 ± 0.044 (12)*	2.81 ± 0.39 (12)	0.170 ± 0.029 (16)*
Glycine, $EC_{50,}$ µM (*n*)	1.224 ± 0.054 (31)	0.131 ± 0.020 (14)*	1.05 ± 0.10 (12)	0.0141 ± 0.0029 (12)*
Proton, % (*n*)	46.4 ± 0.90 (34)	70.5 ± 1.6 (19)*	42.4 ± 2.4 (12)	67.7 ± 2.6 (12)*
Zinc, $IC_{50,}$ nM (*n*)	8.67 ± 0.60 (45)	16.7 ± 2.01(13)*	6.53 ± 1.2 (14)	16.2 ± 3.6 (12)
% Inhibited by zinc (*n*)	35.6 ± 1.5 (45)	47.6 ± 3.0 (13)*	23.5 ± 1.9 (14)*	75.6 ± 2.8 (12)*
Calculated P_{OPEN} (*n*)	0.164 ± .044 (41)	-	0.121 ± .0056 (8)*	-

Table 3

Assay	WT 2A	S810R	S810G	S810N
Glutamate, $EC_{50,}$ µM (*n*)	3.40 ± 0.12 (39)	1.03 ± 0.14 (15)*	2.95 ± 0.28 (12)	2.23 ± 0.20 (12)*
Glycine, $EC_{50,}$ µM (*n*)	1.176 ± 0.041 (36)	0.553 ± 0.059 (11)*	0.994 ± 0.067 (12)	0.868 ± 0.079 (13)
Proton, % (*n*)	44.22 ± 0.66 (33)	52.15 ± 0.85 (14)*	43.0 ± 1.6 (16)	52.7 ± 1.8 (12)*
Zinc, $IC_{50,}$ nM (*n*)	7.40 ± 0.61 (39)	6.45 ± 0.57 (10)	4.64 ± 0.78 (13)	9.9 ± 1.2 (15)
% Inhibited by zinc (*n*)	31 ± 1.9 (45)	32.9 ± 2.6 (10)	22.6 ± 2.3 (13)	36.6 ± 3.3 (15)
Calculated P_{OPEN} (*n*)	0.164 ± .044 (41)	0.1769 ± .00082 (8)	0.0934 ± .0036 (7)*	0.217 ± .036 (5)

Table 4

Assay	WT 2A	Q811R	Q811H	Q811P
Glutamate, $EC_{50,}$ µM (*n*)	3.36 ± 0.15 (44)	2.45 ± 0.19 (16)	2.98 ± 0.26 (12)	10.65 ± 0.49 (17)*
Glycine, $EC_{50,}$ µM (*n*)	1.361 ± 0.036 (46)	0.806 ± 0.043 (12)*	0.948 ± 0.022 (12)*	4.65 ± 0.19 (15)*
Proton, % (*n*)	42.48 ± 0.80 (35)	78.3 ± 2.4 (12)*	46.59 ± 0.61 (12)	24.33 ± 0.80 (16)*
Zinc, $IC_{50,}$ nM (*n*)	5.84 ± 0.47 (41)	13.7 ± 3.0 (12)*	6.57 ± 0.86 (12)	2.68 ± 0.13 (12)*
% Inhibited by zinc (*n*)	30.9 ± 1.7 (41)	70.7 ± 2.9 (12)*	27.8 ± 4.0 (12)	14.8 ± 1.4 (12)*
Calculated P_{OPEN} (*n*)	0.164 ± .044 (41)	0.591 ± .016 (6)*	0.0667 ± .0017 (7)*	-

Table 5.1

Assay	WT 2A	L812V	L812R
Glutamate, $EC_{50,}$ µM (*n*)	3.358 ± 0.095 (85)	0.465 ± 0.035 (14)*	0.715 ± 0.035 (6)*
Glycine, $EC_{50,}$ µM (*n*)	1.81 ± 0.11 (102)	0.192 ± 0.023 (16)*	0.275 ± 0.045 (12)*
Proton, % (*n*)	48.1 ± 1.1 (32)	30.6 ± 1.8 (12)*	24.7 ± 2.6 (12)*
Zinc, $IC_{50,}$ nM (*n*)	6.59 ± 0.86 (14)	5.14 ± 0.60 (12)	7.0 ± 2.0 (8)*
% Inhibited by zinc (*n*)	27.4 ± 3.1 (14)	26.2 ± 2.1 (12)	31.1 ± 4.2 (7)*
Calculated P_{OPEN} (*n*)	0.164 ± .044 (41)	0.0475 ± .0025 (6)*	0.023 ± .010 (7)

Table 5.2

Assay	WT 2A	L812M	L812Q
Glutamate, $EC_{50,}$ µM (*n*)	3.358 ± 0.095 (85)	0.395 ± 0.028 (37)*	0.67 ± 0.09 (8)*
Glycine, $EC_{50,}$ µM (*n*)	1.81 ± 0.11 (102)	0.1378 ± 0.0069 (49)*	0.14 ± 0.01 (14)*
Proton, % (*n*)	48.1 ± 1.1 (32)	83.6 ± 1.5 (7)*	-
Zinc, $IC_{50,}$ nM (*n*)	6.59 ± 0.86 (14)	-	-
% Inhibited by zinc (*n*)	27.4 ± 3.1 (14)	-	-
MTSEA	0.164 ± .044 (41)	-	-

Table 6

Assay	WT 2A	D813N	D813Y	D813E
Glutamate, $EC_{50,}$ µM (*n*)	3.21 ± 0.14 (37)	2.79 ± 0.19 (12)*	1.81 ± 0.017 (12)*	2.67 ± 0.13 (12)*
Glycine, $EC_{50,}$ µM (*n*)	1.288 ± 0.034 (38)	0.530 ± 0.032 (12)*	0.868 ± 0.463 (12)*	0.949 ± 0.050 (12)
Proton, % (*n*)	41.40 ± 0.43 (32)	36.7 ± 1.5 (12)	72.1 ± 1.8 (12)*	50.3 ± 1.6 (12)*
Zinc, $IC_{50,}$ nM (*n*)	7.23 ± 0.59 (36)	4.09 ± 0.32 (10)*	13.57 ± 2.8 (12)	8.58 ± 0.61 (12)*
% Inhibited by zinc (*n*)	28.8 ± 1.5 (36)	29.8 ± 2.2 (10)	66.4 ± 3.9 (12)*	44.5 ± 1.7 (12)*
Calculated P_{OPEN} (*n*)	0.164 ± .044 (41)	0.114 ± .0054 (6)*	0.367 ± .016 (6)*	0.216 ± .009 (4)*

Table 7.1

Assay	WT 2A	I814F	I814N
Glutamate, $EC_{50,}$ µM (*n*)	3.12 ± 0.15 (33)	1.651 ± 0.062 (11)*	1.81 ± 0.17 (12)
Glycine, $EC_{50,}$ µM (*n*)	1.288 ± 0.034 (38)	0.463 ± 0.026 (8)*	0.868 ± 0.046 (12)
Proton, % (*n*)	43.04 ± 0.36 (24)	72.9 ± 2.0 (12)*	71.8 ± 1.6 (12)*
Zinc, $IC_{50,}$ nM (*n*)	8.44 ± 0.72 (38)	12.9 ± 2.3 (12)	13.6 ± 2.8 (12)
% Inhibited by zinc (*n*)	30.1 ± 1.3 (38)	46.6 ± 3.2 (12)	66.4 ± 4.0 (12)*
Calculated P_{OPEN} (*n*)	0.164 ± .014 (41)	0.311 ± .035 (7)*	0.0520 ± .0015 (8)*

Table 7.2

Assay	WT 2A	I814S	I814T
Glutamate, $EC_{50,}$ µM (*n*)	3.12 ± 0.15 (33)	3.77 ± 0.23 (12)	3.03 ± 0.29 (10)
Glycine, $EC_{50,}$ µM (*n*)	1.288 ± 0.034 (38)	1.054 ± 0.030 (13)	1.31 ± 0.19 (12)
Proton, % (*n*)	43.04 ± 0.36 (24)	15.45 ± 0.57 (12)*	30.6 ± 1.4 (12)*
Zinc, $IC_{50,}$ nM (*n*)	8.44 ± 0.72 (38)	3.02 ± 0.18 (12)*	7.28 ± 0.93 (11)
% Inhibited by zinc (*n*)	30.1 ± 1.3 (38)	18.7 ± 3.1 (12)*	34.6 ± 4.8 (11)
Calculated P_{OPEN} (*n*)	0.164 ± .044 (41)	0.049 ± .006 (3)*	-

Table 8

Assay	WT 2A	D815Y	D815G	D815H
Glutamate, $EC_{50,}$ µM (*n*)	3.86 ± 0.14 (34)	4.26 ± 0.15 (12)*	2.79 ± 0.11 (12)*	2.97 ± 0.16 (6)
Glycine, $EC_{50,}$ µM (*n*)	1.209 ± 0.042 (19)	1.237 ± 0.035 (12)	1.201 ± 0.082 (12)	0.873 ± 0.088 (10)
Proton, % (*n*)	42.7 ± 1.2 (28)	20.6 ± 1.7 (14)*	53.4 ± 2.1 (8)*	39.38 ± 0.99 (12)
Zinc, $IC_{50,}$ nM (*n*)	9.74 ± 0.78 (24)	3.83 ± 0.39 (12)*	10.57 ± 0.95 (12)	6.32 ± 0.65 (12)
% Inhibited by zinc (*n*)	36.7 ± 1.6 (36)	17.4 ± 1.48 (12)*	26.7 ± 1.2 (6)*	37.7 ± 3.5 (12)
Calculated P_{OPEN} (*n*)	0.164 ± .044 (41)	0.054 ± .010 (6)*	0.184 ± .010 (6)	0.2561 ± .0079 (7)*

Table 9

Assay	WT 2A	N816T	N816K
Glutamate, $EC_{50,}$ µM (*n*)	3.186 ± 0.098 (55)	1.88 ± 0.11 (14)*	0.360 ± 0.047 (8)*
Glycine, $EC_{50,}$ µM (*n*)	1.223 ± 0.030 (52)	0.419 ± 0.054 (13)*	0.149 ± 0.014 (17)*
Proton, % (*n*)	48.39 ± 0.49 (40)	16.4 ± 1.7 (11)*	30.6 ± 1.8 (13)*
Zinc, $IC_{50,}$ nM (*n*)	8.810 ± 0.593 (43)	2.91 ± 0.28 (12)*	5.11 ± 0.84 (18)*
% Inhibited by zinc (*n*)	30.2 ± 1.1 (55)	10.7 ± 1.2 (12)*	16.9 ± 2.4 (18)*
Calculated P_{OPEN} (*n*)	0.164 ± .044 (41)	0.0089 ± .0032 (7)	0.0385 ± .0020 (6)*

Table 10

Assay	WT 2A	M817V	M817R	M817T
Glutamate, $EC_{50,}$ µM (*n*)	3.62 ± 0.11 (6)	0.28 ± 0.039 (8)*	NE	1.18 ± 1.1 (12)*
Glycine, $EC_{50,}$ µM (*n*)	0.903 ± 0.068 (6)	0.135 ± 0.12 (8)*	NE	0.52 ± 0.12 (12)*
Proton, % (*n*)	41.4 ± 1.3 (9)	89.0 ± 1.5 (8)*	NE	72.1 ± 1.8 (12)*
Zinc, $IC_{50,}$ nM (*n*)	7.9 ± 1.3 (8)	ND	NE	27.9 ± 6.4 (11)*
% Inhibited by zinc (*n*)	36.8 ± 3.2 (8)	31.0 ± 4.8 (7)*	NE	79.0 ± 3.4 (11)*
Calculated P_{OPEN} (*n*)	0.164 ± .044 (41)	-	NE	-

Table 11.1

Assay	WT 2A	A818V	A818P
Glutamate, $EC_{50,}$ µM (*n*)	3.70 ± 0.14 (22)	1.60 ± 0.144 (13)*	0.97 ± 0.056 (12)*
Glycine, $EC_{50,}$ µM (*n*)	0.96 ± 0.045 (33)	0.380 ± 0.026 (13)*	0.270 ± 0.027 (11)*
Proton, % (*n*)	38.4 ± 1.3 (36)	68.6 ± 1.3 (13)*	74.37 ± 0.89 (12)*
Zinc, $IC_{50,}$ nM (*n*)	6.59 ± 0.20 (26)	12.9 ± 2.3 (13)*	8.6 ± 2.3 (13)*
% Inhibited by zinc (*n*)	30.3 ± 1.8 (26)	69.76 ± 8.9 (13)*	44.5 ± 7.1 (12)*
Calculated P_{OPEN} (*n*)	0.164 ± .044 (41)	-	-

Table 11.2

Assay	WT 2A	A818T	A818E
Glutamate, $EC_{50,}$ µM (*n*)	3.70 ± 0.14 (22)	0.704 ± 0.055 (12)*	0.85 ± 0.10 (17)*
Glycine, $EC_{50,}$ µM (*n*)	0.96 ± 0.045 (33)	0.281 ± 0.028 (10)*	0.296 ± 0.020 (17)*
Proton, % (*n*)	38.4 ± 1.3 (36)	80.4 ± 1.4 (12)*	68.2 ± (12)*
Zinc, $IC_{50,}$ nM (*n*)	6.59 ± 0.20 (26)	21 ± 12 (8)*	15.0 ± 3.3 (19)*
% Inhibited by zinc (*n*)	30.3 ± 1.8 (26)	96 ± 3.6 (12)*	72.2 ± 3.3 (19)*
Calculated P_{OPEN} (*n*)	0.164 ± .044 (41)	-	-

Table 12

Assay	WT 2A	G819C	G819S
Glutamate, $EC_{50,}$ µM (*n*)	3.48 ± 0.13 (26)	3.93 ± 0.22 (12)	2.77 ± 0.20 (7)
Glycine, $EC_{50,}$ µM (*n*)	1.031 ± 0.046 (40)	0.68 ± 0.14 (12)	0.87 ± 0.04 (6)
Proton, % (*n*)	46.6 ± 2.0 (28)	21.6 ± 1.7 (12)*	33.1 ± 4.5 (8)
Zinc, $IC_{50,}$ nM (*n*)	6.35 ± 0.58 (28)	1.74 ± 0.15 (13)*	1.86 ± 0.15 (6)*
% Inhibited by zinc (*n*)	36.8 ± 2.5 (28)	9.3 ± 1.1 (13)*	16.5 ± 6.6 (6)
Calculated P_{OPEN} (*n*)	0.164 ± .044 (41)	-	-

Table 13

Assay	WT 2A	V820A	V820E	V820G
Glutamate, $EC_{50,}$ µM (*n*)	3.67 ± 0.17 (16)	4.66 ± 0.31 (12)	3.19 ± 0.24 (12)	2.98 ± 0.14 (12)
Glycine, $EC_{50,}$ µM (*n*)	1.013 ± 0.069 (16)	1.198 ± 0.093(14)	0.635 ± 0.095 (12)*	1.04 ± 0.14 (12)
Proton, % (*n*)	46.6 ± 2.8 (14)	56.7 ± 2.7 (11)	40.6 ± 2.0 (10)	48.4 ± 5.7 (12)
Zinc, $IC_{50,}$ nM (*n*)	7.4 ± 1.1 (14)	16 ± 14 (8)	3.50 ± 0.30 (12)*	8.06 ± 0.83 (12)
% Inhibited by zinc (*n*)	32.6 ± 4.2 (14)	33.5 ± 3.1 (8)	22.3 ± 2.9 (12)	42.8 ± 5.3 (12)*
Calculated P_{OPEN} (*n*)	0.164 ± .044 (41)	-	0.036 ± .015 (6)*	-

Table 14

Assay	WT 2A	F821L	F821C	F821I
Glutamate, $EC_{50,}$ µM (*n*)	3.07 ± 0.14 (36)	2.23 ± 0.32 (6)*	2.1 ± 0.12 (12)*	2.52 ± 0.17 (6)*
Glycine, $EC_{50,}$ µM (*n*)	1.312 ± .039 (37)	0.719 ± 0.037 (12)*	0.732 ± 0.061 (12)*	0.709 ± 0.063 (10)*
Proton, % (*n*)	42.1 ± 1.2 (30)	52.8 ± 2.8 (15)	62.9 ± 2.0 (11)*	53.1 ± 2.9 (15)
Zinc, $IC_{50,}$ nM (*n*)	6.38 ± 0.43 (43)	15.3 ± 6.0 (10)	10.5 ± 2.8 (11)	5.35 ± 0.98 (12)
% Inhibited by zinc (*n*)	30.0± 1.9 (43)	52 ± 10 (11)	58.8 ± 4.1 (11)*	44.4 ± 2.2 (12)*
Calculated P_{OPEN} (*n*)	0.164 ± .044 (41)	-	0.28 ± .05 (3)*	0.23 ± .012 (7)*

Bibliography:

Akgül G, Mcbain CJ, Akgül G, Akgül A, Mcbain CJ (2016) Diverse roles for ionotropic glutamate receptors on inhibitory interneurons in developing and adult brain Excitatory synapses on MGE-derived interneurons Excitatory synapses on CGE-derived interneurons. J Physiol J Physiol.

Alt A, Weiss B, Ogden AM, Knauss JL, Oler J, Ho K, Large TH, Bleakman D (2004) Pharmacological characterization of glutamatergic agonists and antagonists at recombinant human homomeric and heteromeric kainate receptors in vitro. Neuropharmacology.

Amin JB, Salussolia CL, Chan K, Regan MC, Dai J, Zhou HX, Furukawa H, Bowen ME, Wollmuth LP (2017) Divergent roles of a peripheral transmembrane segment in AMPA and NMDA receptors. J Gen Physiol.

Anwyl R (1999) Metabotropic glutamate receptors: Electrophysiological properties and role in plasticity. Brain Res Rev.

Attwell D, Laughlin SB (2001) An energy budget for signaling in the grey matter of the brain. J Cereb Blood Flow Metab.

Auton A et al. (2015) A global reference for human genetic variation. Nature.

Averof M, Rokas A, Wolfe KH, Sharp PM (2000) Evidence for a high frequency of simultaneous double-nucleotide substitutions. Science (80-).

Bomba L, Walter K, Soranzo N (2017) The impact of rare and low-frequency genetic variants in common disease. Genome Biol.

Carvajal FJ, Mattison HA, Cerpa W (2016) Role of NMDA Receptor-Mediated Glutamatergic

Signaling in Chronic and Acute Neuropathologies. Neural Plast.

Carvill GL et al. (2013) GRIN2A mutations cause epilepsy-aphasia spectrum disorders. Nat Genet.

Černý J, Božíková P, Balík A, Marques SM, Vyklický L (2019) NMDA receptor opening and closing-Transitions of a molecular machine revealed by molecular dynamics. Biomolecules Available at: file:///C:/Users/trg/Downloads/biomolecules-09-00546.pdf.

Chang HR, Kuo CC (2008) The activation gate and gating mechanism of the NMDA receptor. J Neurosci.

Chen G, Van Den Pol AN (1998) Coexpression of multiple metabotropic glutamate receptors in axon terminals of single suprachiasmatic nucleus neurons. J Neurophysiol.

Chen TJ, Kukley M (2020) Glutamate receptors and glutamatergic signalling in the peripheral nerves. Neural Regen Res.

Chittajallu R, Vignes M, Dev KK, Barnes JM, Collingridge GL, Henley JM (1996) Regulation of glutamate release by presynaptic kainate receptors in the hippocampus. Nature.

Chuang JH, Li H (2004) Functional bias and spatial organization of genes in mutational hot and cold regions in the human genome. PLoS Biol.

Clements JD, Feltz A, Sahara Y, Westbrook GL (1998) Activation kinetics of AMPA receptor channels reveal the number of functional agonist binding sites. J Neurosci.

Coutinho V, Knöpfel T (2002) Metabotropic glutamate receptors: Electrical and chemical signaling properties. Neuroscientist.

Cull-Candy S, Kelly L, Farrant M (2006) Regulation of Ca2+-permeable AMPA receptors:

synaptic plasticity and beyond. Curr Opin Neurobiol.

David Weaver C, Yao TL, Powers AC, Verdoorn TA (1996) Differential expression of glutamate receptor subtypes in rat pancreatic islets. J Biol Chem.

Davies K (2013) The era of genomic medicine. Clin Med J R Coll Physicians London.

Dewey FE, Pan S, Wheeler MT, Quake SR, Ashley EA (2012) DNA sequencing clinical applications of new DNA sequencing technologies. Circulation.

Dingledine R, Borges K, Bowie D, Traynelis SF (1999) The glutamate receptor ion channels. Pharmacol Rev.

Duzkale H, Shen J, Mclaughlin H, Alfares A, Kelly M, Pugh T, Funke B, Rehm H, Lebo M (2013) A systematic approach to assessing the clinical significance of genetic variants. Clin Genet.

Fernández-Marmiesse A et al. (2019) Rare Variants in 48 Genes Account for 42% of Cases of Epilepsy With or Without Neurodevelopmental Delay in 246 Pediatric Patients. Front Neurosci.

Fernández-Montoya J, Avendaño C, Negredo P (2018) The glutamatergic system in primary somatosensory neurons and its involvement in sensory input-dependent plasticity. Int J Mol Sci.

Gill SS, Pulido OM, Mueller RW, McGuire PF (1998) Molecular and immunochemical characterization of the ionotropic glutamate receptors in the rat heart. Brain Res Bull.

Grados MA, Atkins EB, Kovacikova GI, McVicar E (2015) A selective review of glutamate pharmacological therapy in obsessive–compulsive and related disorders. Psychol Res Behav

Manag.

Grueter BA, Winder DG (2005) Group II and III metabotropic glutamate receptors suppress excitatory synaptic transmission in the dorsolateral bed nucleus of the stria terminalis. Neuropsychopharmacology.

Hamosh A, Scott AF, Amberger J, Valle D, McKusick VA (2000) Online Mendelian Inheritance in Man (OMIM). Hum Mutat.

Hansen KB, Furukawa H, Traynelis SF (2010) Control of assembly and function of glutamate receptors by the amino-terminal domain. Mol Pharmacol.

Hogan-Cann AD, Anderson CM (2016) Physiological Roles of Non-Neuronal NMDA Receptors. Trends Pharmacol Sci.

Hollmann M (1994) Cloned Glutamate Receptors. Annu Rev Neurosci.

Iacobucci GJ, Popescu GK (2018) Kinetic models for activation and modulation of NMDA receptor subtypes. Curr Opin Physiol.

Jimenez-Sanchez G, Childs B, Valle D (2001) Human disease genes. Nature.

Jonas P (2000) The time course of signaling at central glutamatergic synapses. News Physiol Sci.

Kandel ER, Schwartz JH, Jessell TM (2000) Principles of Neural Science, fourth addition.

Karakas E, Simorowski N, Furukawa H (2009) Structure of the zinc-bound amino-terminal domain of the NMDA receptor NR2B subunit. EMBO J.

Karczewski KJ et al. (2019) Variation across 141,456 human exomes and genomes reveals the spectrum of loss-of-function intolerance across human protein-coding genes. bioRxiv.

Kumar A (2015) NMDA receptor function during senescence: Implication on cognitive performance. Front Neurosci.

Kwon JM, Goate AM (2000) The candidate gene approach. Alcohol Res Heal.

Lapidus KAB, Soleimani L, Murrough JW (2013) Novel glutamatergic drugs for the treatment of mood disorders. Neuropsychiatr Dis Treat.

Lee CH, Lü W, Michel JC, Goehring A, Du J, Song X, Gouaux E (2014) NMDA receptor structures reveal subunit arrangement and pore architecture. Nature.

Lek M et al. (2016) Analysis of protein-coding genetic variation in 60,706 humans. Nature.

Li CT, Yang KC, Lin WC (2019a) Glutamatergic dysfunction and glutamatergic compounds for major psychiatric disorders: Evidence from clinical neuroimaging studies. Front Psychiatry.

Li J et al. (2019b) De novo GRIN variants in NMDA receptor M2 channel pore-forming loop are associated with neurological diseases. Hum Mutat.

Ma X, Shao Y, Tian L, Flasch DA, Mulder HL, Edmonson MN, Liu Y, Chen X, Newman S, Nakitandwe J, Li Y, Li B, Shen S, Wang Z, Shurtleff S, Robison LL, Levy S, Easton J, Zhang J (2019) Analysis of error profiles in deep next-generation sequencing data. Genome Biol.

Ménard C, Quirion R (2012) Group 1 metabotropic glutamate receptor function and its regulation of learning and memory in the aging brain. Front Pharmacol.

Monyer H, Burnashev N, Laurie DJ, Sakmann B, Seeburg PH (1994) Developmental and regional expression in the rat brain and functional properties of four NMDA receptors. Neuron.

Monyer H, Sprengel R, Schoepfer R, Herb A, Higuchi M, Lomeli H, Burnashev N, Sakmann B, Seeburg PH (1992) Heteromeric NMDA receptors: Molecular and functional distinction of subtypes. Science (80-).

Myers SJ, Yuan H, Kang JQ, Tan FCK, Traynelis SF, Low CM (2019) Distinct roles of GRIN2A and GRIN2B variants in neurological conditions [version 1; peer review: 2 approved]. F1000Research.

Niciu MJ, Kelmendi B, Sanacora G (2012) Overview of glutamatergic neurotransmission in the nervous system. Pharmacol Biochem Behav.

Nicoletti F, Bockaert J, Collingridge GL, Conn PJ, Ferraguti F, Schoepp DD, Wroblewski JT, Pin JP (2011) Metabotropic glutamate receptors: From the workbench to the bedside. Neuropharmacology.

Niswender CM, Conn PJ (2010) Metabotropic Glutamate Receptors: Physiology, Pharmacology, and Disease. Annu Rev Pharmacol Toxicol.

Papouin T, Ladépêche L, Ruel J, Sacchi S, Labasque M, Hanini M, Groc L, Pollegioni L, Mothet JP, Oliet SHR (2012) Synaptic and extrasynaptic NMDA receptors are gated by different endogenous coagonists. Cell.

Pérez-Otaño I, Larsen RS, Wesseling JF (2016) Emerging roles of GluN3-containing NMDA receptors in the CNS. Nat Rev Neurosci.

Richards S, Aziz N, Bale S, Bick D, Das S, Gastier-Foster J, Grody WW, Hegde M, Lyon E, Spector E, Voelkerding K, Rehm HL (2015) Standards and guidelines for the interpretation of sequence variants: A joint consensus recommendation of the American College of

Medical Genetics and Genomics and the Association for Molecular Pathology. Genet Med.

Rojas A, Dingledine R (2013) Ionotropic glutamate receptors: Regulation by G-protein-coupled receptors. Mol Pharmacol.

Shohami E, Biegon A (2014) Novel Approach to the Role of NMDA Receptors in Traumatic Brain Injury. CNS Neurol Disord - Drug Targets.

Skowrońska K, Obara-Michlewska M, Zielińska M, Albrecht J (2019) NMDA receptors in astrocytes: In search for roles in neurotransmission and astrocytic homeostasis. Int J Mol Sci.

Squire LR (2010) Encyclopedia of Neuroscience.

Strehlow V et al. (2019) GRIN2A -related disorders: Genotype and functional consequence predict phenotype. Brain.

Swanger SA, Vance KM, Pare JF, Sotty F, Fog K, Smith Y, Traynelis SF (2015) NMDA receptors containing the GluN2D subunit control neuronal function in the subthalamic nucleus. J Neurosci.

Swanson CJ, Bures M, Johnson MP, Linden AM, Monn JA, Schoepp DD (2005) Metabotropic glutamate receptors as novel targets for anxiety and stress disorders. Nat Rev Drug Discov.

Toft M (2014) Advances in genetic diagnosis of neurological disorders. Acta Neurol Scand.

Traynelis J, Silk M, Wang Q, Berkovic SF, Liu L, Ascher DB, Balding DJ, Petrovski S (2017) Optimizing genomic medicine in epilepsy through a gene-customized approach to missense variant interpretation. Genome Res.

Traynelis SF, Cull-Candy SG (1990) Proton inhibition of N-methyl-D-aspartate receptors in

cerebellar neurons. Nature.

Traynelis SF, Wollmuth LP, McBain CJ, Menniti FS, Vance KM, Ogden KK, Hansen KB, Yuan H, Myers SJ, Dingledine R (2010) Glutamate receptor ion channels: Structure, regulation, and function. Pharmacol Rev.

Vesikansa A, Sakha P, Kuja-Panula J, Molchanova S, Rivera C, Huttunen HJ, Rauvala H, Taira T, Lauri SE (2012) Expression of GluK1c underlies the developmental switch in presynaptic kainate receptor function. Sci Rep.

Vyklicky V, Krausova B, Cerny J, Ladislav M, Smejkalova T, Kysilov B, Korinek M, Danacikova S, Horak M, Chodounska H, Kudova E, Vyklicky L (2018) Surface expression, function, and pharmacology of disease-associated mutations in the membrane domain of the human GluN2B subunit. Front Mol Neurosci.

Williams MS, Weng C (2019) Genomic Information for Clinicians in the Electronic Health Record. Preprint.

Wu M, Katti P, Zhao Y, Peoples RW (2019) Positions in the N-methyl-D-aspartate Receptor GluN2C Subunit M3 and M4 Domains Regulate Alcohol Sensitivity and Receptor Kinetics. Alcohol Clin Exp Res.

Yang Z, Rannala B (2012) Molecular phylogenetics: Principles and practice. Nat Rev Genet.

Yi F, Zachariassen LG, Dorsett KN, Hansen KB (2018) Properties of triheteromeric N-methyl-D-aspartate receptors containing two distinct GluN1 isoforms. Mol Pharmacol.

Yuan H, Hansen KB, Vance KM, Ogden KK, Traynelis SF (2009) Control of NMDA receptor function by the NR2 subunit amino-terminal domain. J Neurosci.

Zhang Y, Keramidas A, Lynch JW (2016) The free zinc concentration in the synaptic cleft of artificial glycinergic synapses rises to at least 1 µm. Front Mol Neurosci.

Zhou Q, Sheng M (2013) NMDA receptors in nervous system diseases. Neuropharmacology.